Chemical Geology 531 (2020) 119325

Contents lists available at ScienceDirect

Chemical Geology

journal homepage: www.elsevier.com/locate/chemgeo

Effects of magmatic volatile influx in mafic VMS hydrothermal systems: Evidence from the Troodos ophiolite, Cyprus

Andrew J. Martin[a,*], Manuel Keith[b], Daniel B. Parvaz[c], Iain McDonald[a], Adrian J. Boyce[d], Katie A. McFall[a], Gawen R.T. Jenkin[e], Harald Strauss[f], Christopher J. MacLeod[a]

[a] School of Earth and Ocean Sciences, Cardiff University, UK
[b] GeoZentrum Nordbayern, Universität Erlangen- Nürnberg, Germany
[c] Lightning Machines Limited, Grove House, Manchester, UK
[d] Scottish Universities Environmental Research Centre, Glasgow, UK
[e] School of Geography, Geology and the Environment, University of Leicester, UK
[f] Institut für Geologie und Paläontologie, Westfälische Wilhelms-Universität, Germany

ARTICLE INFO

Editor: Catherine Chauvel

Keywords:
VMS
Sulfur isotopes
Magmatic volatile influx
Se/S ratio
Trace elements
LA-ICP- MS

ABSTRACT

The Troodos ophiolite, Cyprus is the principal on- land analogue for mafic-hosted volcanogenic massive sulfide (VMS) deposits. This study, for the first time, presents sulfur isotope ($\delta^{34}S$) data on a regional scale from VMS deposits and other mineralised zones across the Troodos ophiolite. In combination $\delta^{34}S$, Se/S ratios and trace element chemistry (e.g., Se, Cu and Au) of different hydrothermal sulfides are used to assess variations in magmatic volatile influx and the source of metals and sulfur in ancient hydrothermal systems.

Sulfur isotope analyses (n = 180) across 19 mineral deposits indicate a variable source of sulfur in the Troodos VMS hydrothermal system, this in turn allows a variable source of metals to be inferred. Pyrite $\delta^{34}S$ range from −5.5‰ to +13.2‰ with an average of +4.6‰ (n = 160) for all deposits investigated. These $\delta^{34}S$ variations cannot only be explained by variable proportions of thermochemical seawater sulfate reduction ($\delta^{34}S$ +18 to +19‰) and leaching of primary magmatic sulfur from igneous rocks ($\delta^{34}S$ 0-1‰). Consequently, two processes are proposed, explaining the trace metal and $\delta^{34}S$ variation across the Troodos ore-forming systems including, i) a variable source of metals in the sheeted dyke complex and ii) the addition of a magmatic volatile-rich phase to the VMS hydrothermal systems.

Two distinct lava units exist in the Troodos stratigraphy, namely the upper and lower pillow lavas (UPL and LPL). The more primitive UPL are enriched in Au, Se and Cu relative to As, Sb and Zn that are concentrated in the LPL. Some VMS deposits pre-date the formation of the UPL (e.g., Agrokipia A) suggesting Se, Cu and Au depleted source rocks. Hence, the stratigraphic position of VMS deposits and the ratio of UPL:LPL affinity elements (e.g., As + Zn + Sb vs. Cu + Se + Au) imply a systematic relationship between trace element distribution and stratigraphic depth; this relates to the relative proportion of UPL and LPL affinity lavas within the metal source region.

$\delta^{34}S$ values <0‰ recorded in some VMS deposits that are less than the Troodos magmatic mean of 0- 1‰ may be related to anhydrite buffering during fluid ascent, microbial sulfate reduction or the direct contribution of magmatically derived sulfur, to the hydrothermal system from an underlying magma chamber via volatile exsolution. We propose that negative $\delta^{34}S$ values combined with $Se/S \times 10^6$ ratios >500 in pyrite suggest the contribution of a magmatic volatile component (e.g., Apliki and Skouriotissa). We demonstrate that the source of metals and sulfur in the Troodos VMS hydrothermal system is affected by regional scale processes related to i) variable source lithologies and, ii) the contribution of a magmatic volatile phase to some Troodos VMS hydrothermal systems.

1. Introduction

Seafloor hydrothermal systems have been discovered in a range of tectonic settings including mid-ocean ridges (Hannington et al., 1998; Humphris et al., 1995), back-arc spreading centres (Fouquet et al., 1993; Herzig et al., 1998a) and oceanic island arcs (Berkenbosch et al.,

* Corresponding author.
E-mail address: ajmartin@mun.ca (A.J. Martin).

https://doi.org/10.1016/j.chemgeo.2019.119325
Received 15 May 2019; Received in revised form 19 September 2019; Accepted 2 October 2019
Available online 23 October 2019

2012; de Ronde et al., 2005d). Hence, submarine mineral deposits and their ancient on-land VMS analogues are spatially associated with magmatism in convergent and divergent tectonic settings (Franklin et al., 2005; Hannington et al., 2011; Humphris and Klein, 2018). The magmatic activity provides a heat source that drives hydrothermal convection and VMS formation. Seawater is entrained becoming heated to greenschist facies temperatures (~400 °C) at depth in the oceanic crust. The hot and acidic fluid leaches metals from source rocks and transports them to the seafloor, where metal sulfides precipitate upon exhalation and mixing with ambient seawater (Butterfield et al., 1990; German and Von Damm, 2004; Petersen et al., 2000). In areas of sustained fluid flow, massive sulfide deposits form at, or close to the seafloor. These may subsequently be preserved as volcanogenic massive sulfide (VMS) deposits in ophiolite terrains, such as the Troodos ophiolite, Cyprus (Hannington et al., 1998).

The Troodos ophiolite is the principal on-land analogue for mafic, Cyprus-type or Cu-rich VMS mineralisation that formed in an intermediate to slow spreading subduction zone related environment (Allerton and Vine, 1991; Hannington et al., 1998; Varga, 1991). The oceanic crust of the Troodos ophiolite is characterised by an exceptional preservation of seafloor structures including original seafloor sulfide textures that lack evidence of obduction related metamorphic overprinting (Adamides, 2010; Constantinou, 1980; Hannington et al., 2011; Keith et al., 2016a, b). The geochemistry of sulfides in Troodos VMS deposits is comparable to modern seafloor massive sulfide (SMS) deposits, demonstrating that ore forming processes are analogous between actively forming systems and ancient VMS systems preserved on land (Hannington et al., 1998, 2011; Keith et al., 2016a; Martin et al., 2019; Pedersen et al., 2017). In contrast to active SMS systems, ophiolite hosted VMS deposits offer the unique opportunity to study ore forming processes in the third dimension, i.e. with stratigraphic depth (Keith et al., 2016a; Martin et al., 2019; Pedersen et al., 2017). However, direct information on hydrothermal fluid composition is absent in ancient ophiolite terrains making it difficult to assess temporal variations in physicochemical fluid parameters, such as temperature, pH, redox conditions and ligand availability. Instead, trace element geochemistry may be used to constrain variations in ore-forming processes (Grant et al., 2018; Keith et al., 2016a, b; Koschinsky et al., 2008; Maslennikov et al., 2009; Wohlgemuth-Ueberwasser et al., 2015). Additionally, sulfur isotopes ($\delta^{34}S$) and Se/S ratios of sulfides may be used to define the source of sulfur and Se in seafloor and ancient hydrothermal systems (Herzig et al., 1998a; Layton-Matthews et al., 2013; McDermott et al., 2015).

The application of sulfur isotopes and trace element analyses in seafloor hydrothermal systems in a range of tectonic settings provides constraints between magmatic volatile influx, hydrothermal system maturation and fluid evolution (de Ronde et al., 2005d; Herzig et al., 1998a; Sun et al., 2004; Wohlgemuth-Ueberwasser et al., 2015; Yang and Scott, 2002; McDermott et al., 2015). Variation in protolith geochemistry and the ability of melts in arc and back-arc environments to exsolve a magmatic volatile phase can lead to the enrichment of magmatophile trace elements like Au and Cu in subduction related hydrothermal systems (de Ronde et al., 2003d, 2005; Hedenquist and Lowenstern, 1994; Herzig et al., 1998a; Yeats et al., 2014; Patten et al., 2017, 2019; Keith et al., 2018).

Previous sulfur isotope studies on Troodos ophiolite VMS deposits have focused on local scale mound related processes. For example, Keith et al. (2016a) found a systematic relationship between sulfur isotope values in pyrite with stratigraphic depth in the Skouriotissa VMS deposit varying from −1.4‰ to +6.1‰ between deep and shallow stockwork sections, respectively. Pedersen et al. (2017) identified a biogenic sulfur isotope signature in pyrite from the Akaki River section characterised by extremely light $\delta^{34}S$ values in pyrite of - 22‰. Hannington et al. (1998) presented analyses of hydrothermal sulfides from Troodos VMS deposits that range from +1.9‰ to +8.2‰. Sulfur isotope data also exists for a complete section through the Troodos crust with Alt (1994) recording primary magmatic sulfur values of 0-1‰ that become progressively enriched towards heavier values with increasing hydrothermal alteration and mineralisation (e.g., epidosites at +6.2‰).

In this study we present the first extensive $\delta^{34}S$ data for 19 VMS deposits and associated mineralised occurrences across the Troodos ophiolite. Our data shows significant variations in Se/S ratios and magmatophile trace element concentrations (e.g., Cu, Te, Se) on a regional scale. We demonstrate that the $\delta^{34}S$ of hydrothermal sulfides varies between VMS deposits due to both a variable magmatic volatile influx and different proportions of sulfur derived from thermochemical seawater reduction and the leaching of sulfur from igneous host rocks.

2. Geological overview and sample localities

The Cretaceous Troodos ophiolite (92 Ma) formed in a supra-subduction zone setting, most likely in a nascent arc environment (Fonseca et al., 2017; Gass, 1980; Miyashiro, 1973; Pearce and Robinson, 2010; Regelous et al., 2014). Serpentinization initiated differential uplift during the Neogene focused under Mt. Olympus that led to the exposure of a complete, mostly un-deformed ophiolite stratigraphy. Ultramafic mantle rocks, plutonic rocks, sheeted dykes, a transitional basal group horizon and a lower and upper lava unit comprise a complete sequence of oceanic lithosphere (Fig. 1). Massive sulfide deposits outcrop at the periphery of the ophiolite occurring in the extrusive sequence (Fig. 1). The ophiolite is overlain by deep water pelagic sediments such as radiolarian cherts (Robertson, 1977) indicating that shortly after crustal accretion (~8 Ma) Troodos was located below the carbon compensation depth (CCD). During the Cretaceous the CCD is estimated at approximately 3500 m water depth (Tyrrell and Zeebe, 2004), thus the Troodos crust likely formed in a deep water environment (Monecke et al., 2014; Keith et al., 2016a).

Volcanogenic massive sulfides are spatially associated with three structural grabens (Solea, Mitsero and Larnaca) likely representing former seafloor spreading centres (Everdingen et al., 1995; Hurst et al., 1994; Varga and Moores, 1985). The grabens show an approximately N-S extension and can be identified based on inversely dipping sheeted dykes (Fig. 2). The Troodos ophiolite has been divided into (from E-W) the Larnaca, Makheras, Southern Troodos Transform Fault Zone (STTFZ), Mitsero, Solea and Polis structural domains (Fig. 2, Table 1; Varga and Moores, 1985). Normal graben bounding faults channelled fluids forming epidosite zones and widespread spilitisation within the sheeted dyke complex. Epidosite zones are interpreted to be the altered relicts of igneous host rocks leached by hydrothermal fluids to mobilise metals and sulfur responsible for SMS/VMS formation at or near the former seafloor (Jowitt et al., 2012; Patten et al., 2017; Richardson et al., 1987).

Volcanogenic massive sulfide deposits investigated in this study are distributed across the entire Troodos ophiolite, and are therefore representative for a range of regional scale ore-forming processes (Figs. 1 and 2, Table 1; Martin et al., 2019). Deposits range in size from 0.1 Mt to >15 Mt (Hannington et al., 1998) with grades of <0.1 wt. % to 3.8 wt. % Cu (Adamides, 2010; Constantinou and Govett, 1973; Hannington et al., 2011). In some deposits a clear exhalative mound or vent fauna are present providing evidence for deposit formation at the seafloor (Fig. 3A- Skouriotissa; Little et al., 1999; Oudin and Constantinou, 1984). However, due to a long legacy of mining, the exhalative mound is not always preserved. Deposits form at different stratigraphic levels (Table 1) within the extrusive sequence occurring, for example, above the upper pillow lavas overlain by sediments (Fig. 3A, Skouriotissa), at the contact between the lower and upper pillow lava horizons (Fig. 3B, Agrokipia) or at the basal group-lower pillow lava contact (Fig. 3C, Mala) (Table 1).

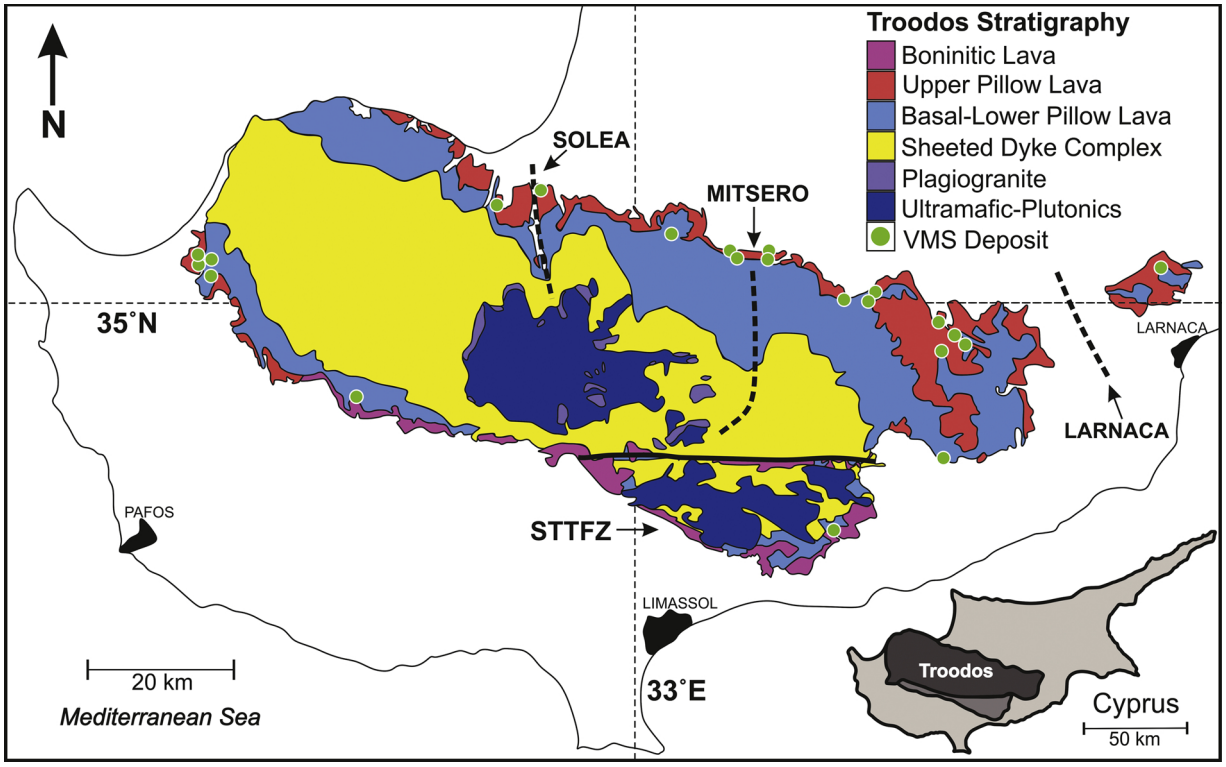

Fig. 1. Simplified geological map of the 92 Myr old Troodos ophiolite, adapted from Martin et al. (2018). Inset location map of the Troodos terrane on the island of Cyprus.

3. Methods

3.1. Trace element geochemistry

Laser Ablation ICP-MS (LA-ICP-MS) was used to determine the *in situ* trace element composition of hydrothermal sulfides (Tables 2–4, n = 250 this study). A combination of spot and line analyses were performed on polished blocks. Prior to LA-ICP-MS analysis, reflected light microscopy was carried out on representative polished blocks to ascertain the modal mineralogy and mineral relationships (see section 4.1). Measurements were carried out at Cardiff University utilising a New Wave Research UP213 UV laser coupled to an iCAP RQ ICP-MS (spot analysis) and a Thermo X-series 2 ICP-MS (line analysis).

Spot analyses were performed with a nominal spot size of 55 µm in time resolved analysis mode at a frequency of 10 Hz. Acquisition lasted 45 s and a gas blank was measured for 20 s prior to laser ablation. For spot analyses the subtraction of gas blanks and internal standard corrections were performed using Thermo Qtegra software. For line analyses the same parameters were employed but acquisition lasted between 80–120 seconds. The beam followed a pre-selected pattern at a scan speed of 6 µm/s aimed to intersect different sulfide phases. Subtraction of gas blanks and internal standard corrections were performed using Thermo Plasmalab software (Prichard et al., 2013; Smith et al., 2014).

Standards used for external calibration include UQAC FeS-1 and in house NiFeS sulfide standards (S, Ni, Fe, and Cu as major elements and Co, Zn, As, Se, Ru, Rh, Pd, Ag, Cd, Sb, Te, Re, Os, Ir, Pt, Au, and Bi as trace elements, cf. Prichard et al., 2013; Smith et al., 2014). The repeated analysis of UQAC FeS-1 during the laser ablation study yielded <10% RSD for Co, As, Se, Ag, Pb and Bi and between 10–18% RSD for Cu, Zn, Sb, Te and Au. RSD for Cd was 26% (See Appendix A2). For all analyses ^{33}S was used as an internal standard. In both instances ^{77}Se was used preferentially over ^{82}Se due to lower interference levels from the Ar-Cl ablation gas. A stoichiometric value of 53.5 wt. % and 35 to 35.5 wt. % for sulfur was used for pyrite and chalcopyrite, respectively, and is within error of measured values for Troodos sulfides (Martin et al., 2019).

3.2. Sulfur isotope analyses

Sulfur isotope ($\delta^{34}S$) analysis was performed at the Natural Environmental Research Council (NERC) stable isotope laboratory at the Scottish Universities Environmental Research Centre (SUERC) and at the Westfälische Wilhelms-Universität, Münster. Subsequently we divide these datasets into dataset A (n = 112), analysed at SUERC and dataset B (n = 68) analysed at Münster (see Appendix A1). For dataset A, pyrite, chalcopyrite and covellite were analysed. In situ measurements were performed by laser combustion combined with conventional sulfur extraction of mineral separates. The methodology for dataset B is outlined by Keith et al. (2016a), a summary is provided below.

Laser combustion analyses were performed on polished blocks that were inserted into a sample chamber, and air was evacuated and subsequently filled with an excess of oxygen (Fallick et al., 1992). Dependant on sulfide grainsize, individual grains with a cumulate area of 100–300 µm were analysed and for sulfides <100 µm, a composite of smaller grains were analysed. The sulfide was combusted using a Spectron Lasers 902Q CW Nd:YAG laser (1 W power), operating in TEM_{00} mode. Further details on system design, laser characteristics and experimental conditions are described in Kelley and Robinson (1990) and Wagner et al. (2002) . The released SO_2 gas from each ablation was then purified in a miniature vacuum line utilising an aceton- CO_2 slush trap to remove water and a standard n-pentane trap to separate SO_2 from CO_2 (Smith et al., 2016). Systematic $\delta^{34}S$ fractionation of the SO_2 during laser ablation was corrected by fractionation factors established for the SUERC facility: chalcopyrite +0.7‰ and pyrite +0.8‰ (Kelley and Robinson, 1990).

Samples analysed via conventional sulfur extraction were either micro- drilled or individual sulfide grains were optically picked. Each analysis used approximately 4–5 µg of sample that was subsequently converted to SO_2 by combustion with 200 µg of cuprous oxide following

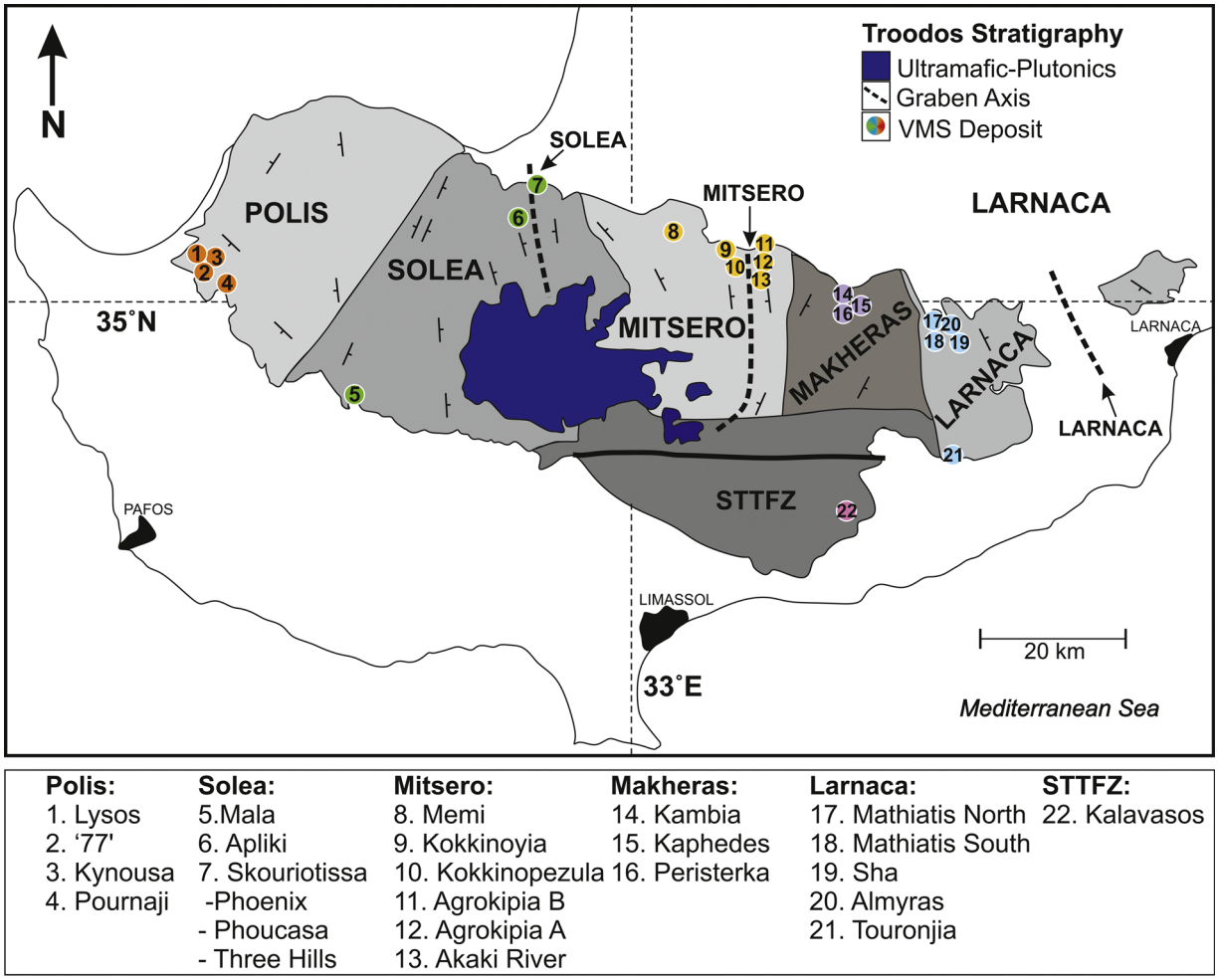

Polis:	Solea:	Mitsero:	Makheras:	Larnaca:	STTFZ:
1. Lysos	5.Mala	8. Memi	14. Kambia	17. Mathiatis North	22. Kalavasos
2. '77'	6. Apliki	9. Kokkinoyia	15. Kaphedes	18. Mathiatis South	
3. Kynousa	7. Skouriotissa	10. Kokkinopezula	16. Peristerka	19. Sha	
4. Pournaji	-Phoenix	11. Agrokipia B		20. Almyras	
	- Phoucasa	12. Agrokipia A		21. Touronjia	
	- Three Hills	13. Akaki River			

Fig. 2. Map with simplified structural domains after Varga and Moores (1985). Different structural domains (grey shaded areas) are defined through structural analysis of the sheeted dyke complex. Coloured dots refer to the investigated VMS deposits within the different structural domains. Skouriotissa comprises three individual ore bodies; Phoenix, Phoucasa and Three Hills. STTFZ = Southern Troodos Transform Fault Zone.

the methodology of Robinson and Kusakabe (1975) .

All samples were analysed using a VGA SIRA II gas source mass spectrometer at SUERC. Values are calculated relative to the Vienna-Canyon Diablo Troilite (V-CDT) reference material and are reported in standard notation. Reproducibility of the results was monitored through the repeated analysis of standards NBS-123 (+17.1‰), IAEA-S-3 (-31.5‰), and SUERC's internal standard CP-1 (−4.6‰). The reproducibility of standards for all analyses in dataset A was better than ±0.7‰ (1σ)(Appendix A1).

For dataset B (n = 68) sulfur isotope analysis was performed on pure mineral separates. Between 70–100 μg of pyrite and 300–500 μg of V_2O_5 was analysed in tin capsules using a Carlo Erba elemental analyser coupled to a ThermoFinnigan Delta plus isotope ratio mass spectrometer (Keith et al., 2016a). All results are reported in standard notation to V-CDT. Reproducibility for dataset B is reported as better than ±0.3‰ (1σ) (Keith et al., 2016a).

4. Results

4.1. Ore mineralogy and petrography

Samples have been classified based on their mineralogy and morphology into massive, semi-massive, stockwork and South Apliki Breccia Zone type. Representative photomicrographs of each sample type are shown in Fig. 4. Massive samples are characterised by >90% sulfide, with interstitial to crudely banded chalcopyrite (Fig. 4A). At Apliki, dendritic pyrite forms bands with coarse interlocking euhedral grains towards the base (Fig. 4B). Semi-massive samples contain <90% sulfide with minor Fe-oxide, covellite and silica (Fig. 4C and D). Stockwork samples consist of discrete veins of silica, pyrite, chalcopyrite and sphalerite (Fig. 4E). South Apliki Breccia Zone samples (see Martin et al., 2018) contain coexisting hematite, chalcopyrite and pyrite (Fig. 4F). In combination, these samples represent a wide range of ore-forming processes from the shallow near-seafloor VMS stratigraphy (Fig. 4A) to the lower stockwork zone (Fig. 4E).

4.2. Trace element geochemistry

In this study we present *in situ* trace element chemistry of pyrite (n = 191; Table 2, Fig. 5), chalcopyrite (n = 51; Table 3) and covellite (n = 8; Table 4). Trace element concentrations in sulfides from the Troodos VMS deposits are highly variable. For example, Se in pyrite varies over two orders of magnitude between different VMS deposits from 10.1 to 4513 ppm (Table 2). Concentrations of Te, Co, Bi, Sb and Zn in chalcopyrite are similar or lower than in pyrite, whereas Se is generally enriched in chalcopyrite (Table 2 and 3). Covellite contains appreciable Se reaching 4310 ppm (n = 4, Table 4) and elevated concentrations of Ag, As, Zn and Bi, as well as minor Au (Table 4). Variation in sulfide trace element chemistry is noted on a regional scale between different structural domains (Fig. 5). Correlation (linear R values) between elements in pyrite are limited with the exception of a minor correlation between Bi-Te (R = 0.56), Au-Ag (R = 0.57) and Cd-

Table 1
Summary of sample localities and stratigraphic depth of VMS deposits. All coordinates given in WGS 1984 (36S). *Skouriotissa, Phoucasa deposit.

Deposit	(WGS 1984) N	E	Description	Stratigraphic position
Polis Domain				
Lysos	45536	3877125	VMS	UPL-LPL
77'	45404	3877993	VMS	LPL
Kynousa	45555	3876810	VMS	TOP OF UPL
Pournaji	45536	3876197	VMS	LPL
Solea Domain				
Mala	47046	3864224	VMS	BG-LPL
Apliki	48573	3881812	VMS	LPL
Skouriotissa	49018	3884032	VMS	TOP OF UPL*
Mitsero Domain				
Memi	50366	3877476	VMS	LPL
Kokkinoyia	50974	3877992	VMS	UPL-LPL
Kokkinpozeula	51038	3877259	VMS	LPL
Agrokipia A	51336	3878056	VMS	UPL-LPL
Agrokipia B	/	/	VMS	LPL
Akaki River	51641	3878541	Disseminated/ veins	N/A
Makheras Domain				
Kambia	52473	3873019	VMS	LPL
Kaphedes	52394	3871610	VMS	BG-LPL
Peristerka	52151	3872174	VMS	BG-LPL
Larnaca Domain				
Mathiatis North	53185	3870606	VMS	UPL-LPL
Mathiatis South	53170	3867617	VMS	UPL-LPL
Sha	53421	3867790	VMS	UPL-LPL
Almyras	55390	3870761	Disseminated/ veins	BG
Touronja	53242	3856597	Low T silica-rich	BG-LPL
STTFZ				
Kalavasos	52356	3850308	VMS	UPL-LPL

Zn (R = 0.64). In chalcopyrite, a moderate positive correlation is observed between Au-Te (R = 0.68) and Cd-Ag (R = 0.88) (Appendix A3).

Ratios of Se/S, expressed as Se/S × 10^6 in pyrite (this study, n = 191; Martin et al., 2018, 2019 n = 1323) from different VMS deposits vary between structural domains (Figs. 2 and 6). Pyrite from deposits of the Solea domain, excluding the Apliki VMS deposit, shows the highest average Se/S × 10^6 ratio of 480 (n = 362), whereas the Larnaca domain averages 89 (n = 350). Analyses also indicate a large variation in Se/S ratios in pyrite within individual structural domains; at Solea Se/S × 10^6 ratios range from 3 to 3650 (Fig. 6).

4.3. Sulfur isotope analysis

Sulfur isotope analysis was performed on pyrite (n = 160), chalcopyrite (n = 15) and covellite (n = 5) from 19 VMS deposits and mineralised zones across all structural domains (Fig. 2, Table 5). The average $\delta^{34}S$ value for all samples regardless of the mineral analysed was +4.6‰. Values in pyrite range from -5.5‰ to +13.2‰ (Fig. 7). Pyrite from deposits of the Larnaca domain exhibit the lowest average $\delta^{34}S$ value at +3.4‰ (n = 55) and the STTFZ the highest at +8.0‰ (n = 18) (Table 5). Analyses of chalcopyrite and covellite yield values indistinguishable from pyrite with $\delta^{34}S$ ranging from +0.6 to +5.6‰ and +3.7 to +5.3‰, respectively (Table 5). Results obtained in this study are comparable to those reported in previous studies (Figs. 7 and 8). In some instances, clear populations are identified, for example in the STTFZ (Fig. 8E) where $\delta^{34}S$ values cluster around +2 to +3‰ and +11 to +13‰.

5. Discussion

5.1. Trace element variation

The incorporation of trace elements into hydrothermal sulfides is controlled by physicochemical fluid parameters, such as temperature, fO_2 and pH (Berkenbosch et al., 2012; Huston et al., 1995; Keith et al., 2016a, b; Maslennikov et al., 2009; Wohlgemuth-Ueberwasser et al., 2015). Since the fluid composition responsible for the formation of the Troodos VMS deposits is unknown, mineralogy and mineral chemistry are interpreted as an indirect proxy (Keith et al., 2016a, b; Wohlgemuth-Ueberwasser et al., 2015). The trace element composition of pyrite varies between different structural domains (Fig. 5), some domains are enriched in elements of magmatic affinity (e.g., Solea), such as Se, Cu, Au and Te, whilst others are depleted (e.g., Makheras). Data from the Apliki VMS deposit is presented as a sub-class with respect to the Solea domain, since previous studies have identified Apliki as being unusually enriched in Se due to seafloor oxidation processes (Fig. 5 and 6) (Martin et al., 2018). The highest average Se concentrations in pyrite (excluding Apliki) were identified in the Solea domain at 257 ppm (n = 366,) compared to 47 ppm Se (n = 89) at Larnaca representing the lowest average concentrations. In contrast, As and Sb are enriched in pyrite from the Makheras and STTFZ domains relative to Solea (Fig. 5). We propose that trace element variations between VMS deposits and structural domains are due to different physicochemical fluid conditions (e.g., temperature) during mineralisation or caused by compositional variations in the metal source on a regional scale.

5.2. Linking source rock and VMS composition

The Troodos extrusive sequence contains two distinct lava suites; the upper pillow lavas (UPL) and lower pillow lavas (LPL) (Malpas and Langdon, 1984; Schouten and Kelemen, 2002). The UPL are largely basaltic to picritic in composition with low TiO_2 (<0.4 wt.%) whilst the LPL are basaltic-andesites with high TiO_2 >0.8 wt.% (Robinson and Malpas, 1990). The LPL represent the main 'on axis' accretionary phase and were erupted by frequent, relatively high viscosity eruptions. In contrast, the UPL were erupted in temporally distinct, high volume eruptions (Schouten and Kelemen, 2002).

Volcanogenic massive sulfide deposits form throughout the extrusive sequence of the Troodos ophiolite either overlying the UPL or at the LPL-UPL or basal group-LPL contact (Adamides, 2010; Constantinou and Govett, 1973; Martin et al., 2019). The location of the VMS deposits with respect to the lava stratigraphy has important implications for the source characteristics of different trace metals, as it determines the timing of VMS formation relative to the eruption of the UPL and LPL (cf. Section 5.4). The Agrokipia A deposit (Mitsero domain, Fig. 3B) is overlain by unaltered UPL, therefore demonstrating that UPL accretion post-dates VMS formation at Agrokipia A. In other areas, VMS mineralisation occurs above the UPL sequence where VMS are directly overlain by umber and calcareous sediments (e.g., Skouriotissa, Fig. 3A). In contrast, the Mala deposit represents an example from the basal group-LPL contact suggesting it formed relatively early in the extrusive history of the Troodos ophiolite (Fig. 3C).

Patten et al. (2017) demonstrate that the UPL and LPL contain distinctly different trace element signatures. For example, As, Zn and Sb are incompatible and become preferentially enriched with increasing fractionation at low MgO contents in the LPL (<3.5 wt.%). Concentrations of compatible trace elements, such as Cu, Au and Se are highest prior to magnetite saturation at about 3.5 wt.% MgO (Jenner et al., 2010; Patten et al., 2017); therefore the highest Au, Se and Cu concentrations were reported in the most primitive UPL samples.

Epidosite zones and spilitisation within the sheeted dyke complex are widely accepted as the primary metal source for the hydrothermal systems hosted in the Troodos ophiolite (Jowitt et al., 2012; Patten

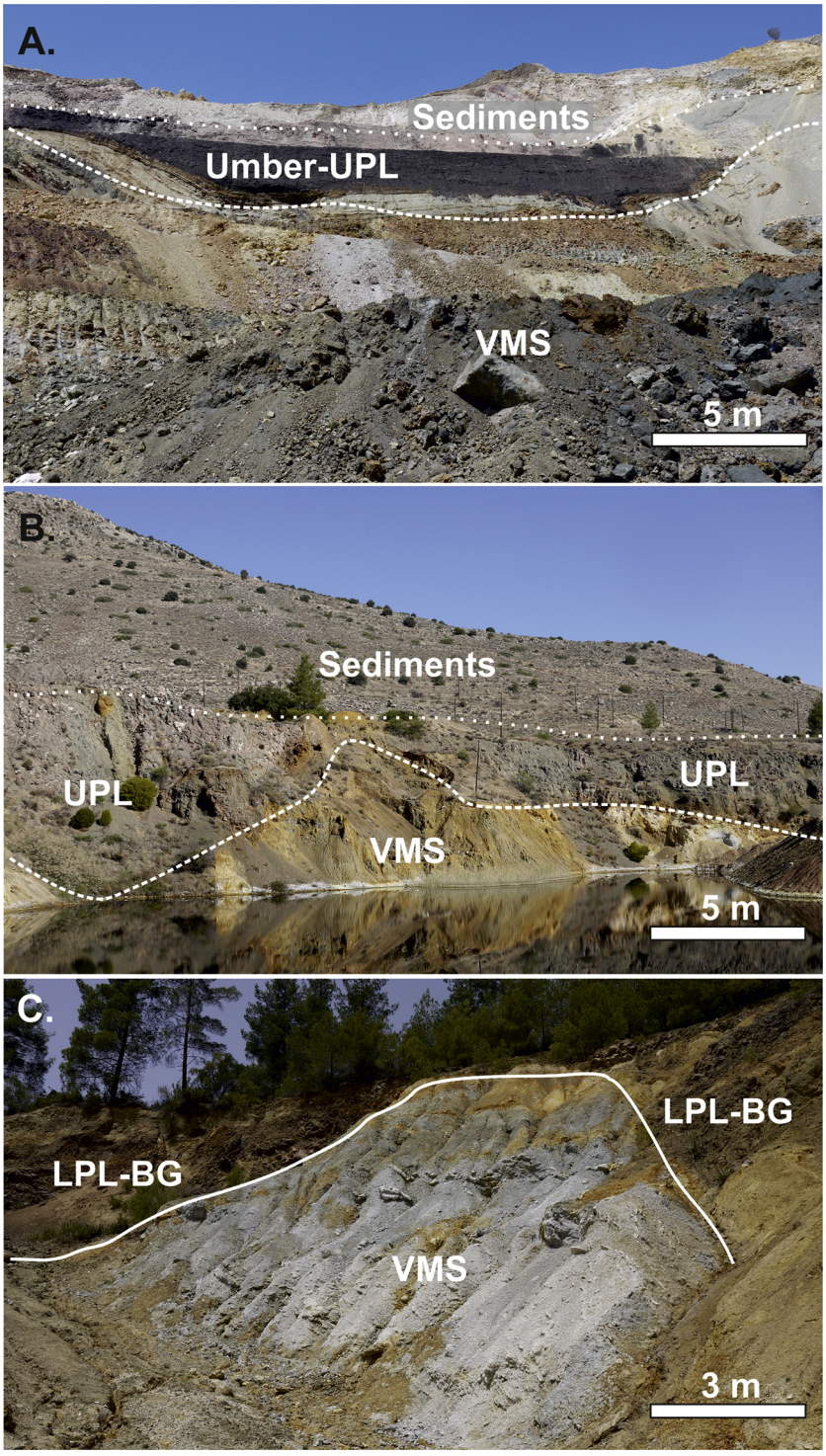

Fig. 3. Field photographs demonstrating key relationships between mineralisation, lava and sediments: (A) Phoucasa, Skouriotissa VMS, massive sulfide overlain directly by umber and calcareous sediment, (B) the Agrokipia A VMS located at the contact between LPL and unaltered UPL that are overlain by calcareous sediments, (C) the Mala VMS mound overlain by flows of the LPL. Mala is located at the base of the LPL at the BG-LPL transition.

et al., 2017; Richardson et al., 1987). Mass balance calculations indicate that 88 ± 16% Au, 91 ± 20% Se and 84 ± 18% Cu has been leached from the metal depleted epidosite zones relative to cogenetic fresh volcanic glass (Jowitt et al., 2012; Patten et al., 2017). The amount of metals mobilised from 5 km^3 of epidosites and 5.9 km^3 of 'altered' sheeted dykes is enough to supply a VMS district, making the assumption that the analysed metals in pyrite are mostly sourced from leaching of the underlying sheeted dyke complex (e.g., Solea domain: Apliki, Mavrovouni, Skouriotissa; Patten et al., 2017).

The UPL:LPL ratio defined by the concentration of Au + Se + Cu (UPL affinity) to As + Zn + Sb (LPL affinity) in hydrothermal pyrite is used to estimate the relative contribution of these metals from UPL and LPL affinity dykes within epidosite zones (or the wider sheeted dyke complex) to the VMS hydrothermal system. Deposits situated in the lower stratigraphy (basal group and LPL) predating UPL accretion are expected to contain lower Au, Se and Cu relative to those that post-date

Table 2
Summary of LA-ICP-MS pyrite data from the investigated VMS deposits. Blank cells represent analyses below the minimum detection limit. Full data and detection limits are presented in Appendix A2.

Deposit	Pyrite	Co ppm	Cu %	Zn ppm	As ppm	Se ppm	Ag ppm	Cd ppm	Sb ppm	Te ppm	Au ppm	Pb ppm	Bi ppm
Agrokipia A	Average	58.7	0.03	1070	1013	351	1.3	3.1	2.7		0.62	14.5	
n = 12	Max	182	0.04	5194	6251	449	5.1	5.9	4.9		1.6	25.2	
	Min	3.03	0.01	>0.01	12.7	279	0.39	0.72	1.1		0.21	4.9	
	Median	47.8	0.03	560	307	324	0.92	3.1	2.4		0.52	12.6	
	σ	53.5	0.01	1541	1806	71.8	1.4	1.9	1.2		0.35	6.5	
Agrokipia B	Average	387	0.03	408	81.7	30.5	2	2.3	2.4	6.00	0.18	145	6.8
n = 10	Max	1151	0.06	1492	608	65.9	3.8	3.9	4.5	27.1	0.18	411	28.2
	Min	3.3	>0.01	25.9	1.1	10.1	0.26	0.30	0.2	0.38	0.18	3.6	0.08
	Median	232	0.03	65.2	4.2	28.1	2	2.8	2.4	2.5	0.18	19.2	1.3
	σ	420	0.02	569	188	17	1.8	1.5	2.2	8.1		189	10.9
Kokkinopezula	Average	59.7	0.05	2749	487	486	4.7	4.6	38.9	6.4	1.3	56.2	1.5
n = 18	Max	215.6	0.36	9390	1103	1371	11.0	11.3	98.9	11.4	10.6	103	4.2
	Min	4.1	>0.01	44.1	40.0	25.3	0.30	0.30	2.3	1.2	0.07	11.3	0.06
	Median	98.3	0.01	92.3	5.3	20.2	0.65	0.5	0.35	17.6	0.07	5	5.3
	σ	82.8	0.1	3864	375	626	3.0	4.8	34.5	4.2	2.6	32.4	1.6
Kokkinoyia	Average	111	0.13	6708	278	297	3.3	5.7	22.5	14.6	1.3	64.1	9.5
n = 43	Max	797	1.7	62591	1103	1371	11	15.8	117	88.4	10.6	232.4	96.1
	Min	4.1	>0.01	15.5	2.3	18.2	0.27	0.26	0.47	1.2	0.01	2.9	0.06
	Median	56	0.03	659.4	185.1	93.9	1.9	4.6	7.5	4.2	0.26	55	2.1
	σ	167	0.3	14003	287	387	3	4.9	32.4	19	1.9	51.8	18.8
Apliki	Average	127	0.31	337	134	1297	0.36	1.1	2.4	6.8	0.19		1
n = 84	Max	447	2.2	4307	1151	4513	0.69	1.2	6	32.5	1.3		6.1
	Min	2.3	>0.01	15.6	2.8	14.4	0.21	1.1	0.3	0.71	0.02		0.03
	Median	98.4	0.09	32.8	85.2	1217	0.31	1.1	2.5	5.1	0.07		0.8
	σ	108	0.5	948	183	954	0.15	0.08	1.7	5.9	0.27		1.2
Skouriotissa	Average	393	0.4	2917	48.7	397	1.4		1.3	17.3	0.37		1.5
n = 22	Max	2289	1.9	23954	130.1	2430	7.1		3.1	82	0.86		4.5
	Min	2.9	0.02	43	3.1	17.8	0.23		0.3	2.6	0.02		0.05
	Median	184	0.21	474.6	44.4	226.7	0.56		0.78	12.4	0.32		1.1
	σ	557	0.56	6312	40.2	600	1.9		1	18.2	0.29		1.3
Kampia	Average	4.7		17	7.2	23.4						260	0.3
n = 2	Max	4.7		17	7.2	23.4						260	0.4
	Min	4.7		17	7.2	23.4						260	0.2
	Median	4.7		17	7.2	23.4						260	0.3
	σ												0.1

the UPL formation (Fig. 9). For all VMS deposits, UPL:LPL ratios range from 0.01 at Agrokipia A to 7.63 at Mala (Table 6A).

This has important implications for the distribution of trace elements in the Troodos VMS deposits. The sheeted dyke complex links the plutonic section, i.e. former magma chambers and the extrusive sequence at the former seafloor, therefore UPL and LPL affinity dykes are discernible within the sheeted dyke complex (Baragar et al., 1990; Staudigel et al., 2000). We propose that an epidosite zone with a relatively high volume of UPL affinity dykes would produce a VMS deposit with elevated concentrations of Au, Se and Cu (Fig. 9). In contrast, a zone comprised solely of andesitic LPL affinity dykes would form a VMS deposit relatively enriched in As, Zn and Sb (Fig. 9) (Patten et al., 2017; Staudigel et al., 2000). Ultimately the relative enrichment in UPL affinity elements relates to the timing of VMS formation relative to lava eruption; VMS deposits that postdate the eruption of the UPL are enriched in Au, Se and Cu (e.g. Skouriotissa, Phoucasa) relative to those within the LPL's (Fig. 9). Consequently, the broad correlation between UPL:LPL ratio and stratigraphic depth suggest that on a regional scale source rock composition may influence the trace metal budget of VMS deposits (Fig. 9). However, significant variations were observed in deposits that formed at the same stratigraphic level, for example Mala and Kaphedes both occur at the basal group-LPL contact but exhibit distinctly different UPL:LPL ratios of 7.63 and 0.35, respectively (Table 6A).

Our model predicts that the ratio of UPL affinity elements (Cu + Se + Au) to LPL affinity elements (Zn + Sb + As) will vary independently from $\delta^{34}S$ values in VMS sulfides; the source of sulfur leached from the UPL and LPL respectively, remains constant at 0-1‰ (Alt, 1994). If this

Table 3
Summary of LA-ICP-MS chalcopyrite data from the investigated VMS deposits. Blank cells represent analyses below the minimum detection limit. Full data and detection limits are presented in Appendix A2.

Deposit	Chalcopyrite	Co ppm	Cu %	Zn ppm	As ppm	Se ppm	Ag ppm	Cd ppm	Sb ppm	Te ppm	Au ppm	Pb ppm	Bi ppm
Apliki	Average	14.0	26.8	262	261	2415	1.5	1.5	5.6	8.3	0.29		0.6
n = 19	Max	34.1	32.7	1193	1270	4517	3.8	2.1	16.8	43.4	1.5		2.7
	Min	3.3	20.2	56.0	5.8	281	0.23	0.87	0.53	0.13	0.02		0.01
	Median	6.5	27.3	154	110	2436	0.89	1.8	4.0	2.9	0.06		0.23
	σ	11.4	2.8	257	364	1162	1.3	0.53	5.2	13.7	0.47		0.80
Skouriotissa	Average	117	22.7	5789	3.3	342	4.5	17.3	0.90	7.1	0.24		0.55
n = 9	Max	378	28.5	18864	3.9	1549	11.6	109	1.0	39.7	0.26		3.5
	Min	2.2	16.7	392	2.7	19.9	0.24	1.1	0.75	0.5	0.22		0.05
	Median	44	24.4	5990	3.3	37	2.2	2.2	0.90	1.2	0.24		0.12
	σ	152	4.3	5252	0.6	574	4.6	37.6	0.15	12.6	0.02		1.1

Table 4
Summary of LA-ICP-MS covellite data from the investigated VMS deposits. Blank cells represent analyses below the minimum detection limit. Full data and detection limits are presented in Appendix A2.

Deposit	Covellite	Co ppm	Cu %	Zn ppm	As ppm	Se ppm	Ag ppm	Cd ppm	Sb ppm	Te ppm	Au ppm	Pb ppm	Bi ppm
Apliki	Average		52.1	257	365	3254	16.7	1.8	15.0	6.0	0.2		8.3
n = 2	Max		52.8	275	439	4310	29.4	1.8	29.2	9.3	0.3		16.3
	Min		51.5	238	290	2197	4.0	1.8	0.8	2.7	0.1		0.3
	Median		52.1	257	365	3254	16.7	1.8	15.0	6.0	0.2		8.3
	σ		0.7	18.7	74.3	1057	12.7	0.0	14.2	3.3	0.1		8.0
Skouriotissa	Average	135	46.2	2650	83.9	1073	8.4		3.3	24.6	0.38	0.0	2.6
n = 2	Max	191	50.9	4369	108.7	1321	12.8		5.0	29.5	0.46	0.0	2.8
	Min	78.6	41.4	930	59.1	826	4.1		1.6	19.7	0.30	0.0	2.4
	Median	135	46.2	2650	83.9	1073	8.4		3.3	24.6	0.38	0.0	2.6
	σ	56.3	4.7	1720	24.8	247	4.3		1.7	4.9	0.08	0.0	0.18

is true then comparing VMS that postdate (e.g. Skouriotissa) and predate the eruption of the UPL (e.g. Mathiatis North) should exhibit different trace element signatures; Skouriotissa should be enriched in Cu, Se and Au relative to Mathiatis North. Skouriotissa contains a total of 1381 ppm UPL affinity elements in pyrite compared with just 482 ppm at Mathiatis North (Table 6A). Sulfur isotope values between the two deposits are comparable at +5.1‰ and +4.4‰ for Skouriotissa and Mathiatis North, respectively. This demonstrates that the stratigraphic depth of VMS mineralisation and its relationship to the UPL's is important in controlling trace element enrichment in some deposits (Fig. 9). The high UPL:LPL ratio reported for Mala (7.63; Table 6A) could suggest an additional source of magmatophile elements (e.g., Au, Se, Cu) as Mala forms deep in the extrusive sequence and therefore did not experience an additional source of Au, Se and Cu from the leaching of UPL affinity protoliths. Instead, we suggest that the contribution of a magmatic volatile component during the early stages of crustal accretion could explain the observed metal enrichment at Mala.

5.3. Selenium/sulfur ratios in Troodos VMS

The Se/S ratio is commonly used in hydrothermal ore deposits as a tracer of magmatic volatile influx (Hannington et al., 1999; Huston et al., 1995; Layton-Matthews et al., 2008, 2013; Martin et al., 2019). In a previous study, we propose that the magmatic volatile influx between the Mitsero and Solea structural domains is distinct, with a stronger magmatic volatile contribution to the latter (Martin et al., 2019). Layton-Matthews et al. (2008, 2013) state that $Se/S \times 10^6$ ratios >500 represent an increased magmatic volatile component in the VMS hydrothermal systems. In this study, combined with previously published data (Martin et al., 2019), we present new Se/S ratios in pyrite (n = 191) representing six structural domains in the Troodos ophiolite (Fig. 6).

Pyrite from Skouriotissa and Apliki (both Solea domain) has maximum $Se/S \times 10^6$ ratios above the magmatic threshold (>500) at about 2380 and 3650, respectively, which could be interpreted as an increased magmatic influx (Layton-Matthews et al., 2008; Martin et al., 2019). Selenium/sulfur ratios clearly demonstrate variations across different VMS deposits and their corresponding structural domains (Figs. 5 and 6). With respect to the Se/S ratios in pyrite, the VMS deposits of the Larnaca domain experienced the lowest magmatic influx, if any, as indicated by the lowest average $Se/S \times 10^6$ ratios of 89 in pyrite (n = 350). This suggests that the magmatic volatile influx varied spatially between VMS deposits and districts across the Troodos ophiolite, which would also result in $\delta^{34}S$ variations on the deposit and district scale.

5.4. Variation in sulfur isotopes

Sulfur from multiple sources incorporated into hydrothermal sulfides has been suggested for modern SMS and ancient VMS systems (McDermott et al., 2015; Ono et al., 2007). These include the biogenic/bacterial (<120 °C) or thermochemical reduction of seawater sulfate (>160 °C), sediment interaction, leaching from igneous rocks and the direct contribution of magmatic volatiles (Berkenbosch et al., 2012; Herzig et al., 1998a; Ono et al., 2007; Pedersen et al., 2017). Primary Troodos magmatic sulfides have a $\delta^{34}S$ value of 0-1‰ (Alt, 1994), whilst Cretaceous seawater has a $\delta^{34}S$ value of +18 to +19‰ (Kampschulte and Strauss, 2004). Modern SMS systems along sediment-starved mid-ocean ridges typically show $\delta^{34}S$ values between 0‰ and +21 to +22‰, with most values between 0-10‰ in sulfides, indicating a variable source of sulfur derived from thermochemical seawater reduction and leaching of magmatic host rocks in variable proportions. During hydrothermal alteration of the Troodos crust, seawater derived fluids become heated and reduced in the subsurface leading to the thermochemical reduction of seawater sulfate at temperatures >160 °C (e.g., Machel, 2001). Bacterial sulfate reduction of seawater at lower temperatures (<120 °C) in an open system can lead to sulfide precipitates with extremely light $\delta^{34}S$ signatures reaching -43.5‰ (Pedersen et al., 2017; Rouxel et al., 2008; Seal, 2006). At higher temperatures light sulfur isotope values <0‰ may also form due magmatic SO_2 that subsequently disproportionates to H_2S and SO_4^{2-}; the former being incorporated in the sulfide precipitates (e.g. Alt et al., 1998; Herzig et al., 1998a; de Ronde et al., 2005d).

Sulfur isotope data from Troodos VMS sulfides presented in this study range from -5.5‰ to +13.2‰ in pyrite (n = 160, Av.= +4.7‰), +0.6‰ to +5.6‰ in chalcopyrite (n = 15, Av.= +3.4‰) and +3.7‰ to +5.3‰ in covellite (n = 5, Av.= +4.5‰) (Fig. 7). This range is similar to that observed in modern sediment-starved seafloor sulfides from subduction zone-related hydrothermal systems (Fig. 10). For example, $\delta^{34}S$ values for modern seafloor sulfides in the Lau back-arc basin range from -7.7‰ at Hine Hina to +16.2‰ at Vai Lili (Herzig et al., 1998a). In contrast, $\delta^{34}S$ in pyrite from the TAG hydrothermal field at the Mid-Atlantic Ridge average +6.4‰ without any negative values (Fig. 10; Herzig et al., 1998b). These variations highlight the variable sources of sulfur in active hydrothermal systems and their fossil VMS counterparts, such as those preserved in the Troodos stratigraphy (Fig. 10).

The Troodos ophiolite formed in a sediment starved supra-subduction zone spreading environment, therefore a sedimentary source of sulfur is unlikely (Gass, 1980; Robertson, 2002, 1975). Evidence of bacterial seawater sulfate reduction are preserved in pyrite from the Akaki River section (Troodos) that exhibit a bacterial $\delta^{34}S$ signature of -21 to - 22‰ related to 'off axis' fluid recharge (Pedersen et al., 2017). Given the higher fluid temperatures of the VMS hydrothermal systems (>200 °C) and the sediment and organic poor environment of Troodos, biogenic seawater sulfate reduction was probably a minor component in the high temperature discharge zones. This is confirmed by Pedersen et al. (2017) for the Agrokipia VMS deposit, where limited $\Delta^{33}S$ values of up to 0.22‰ in pyrite signify a minor biogenic component. However, more extensive biogenic seawater sulfate reduction may have been

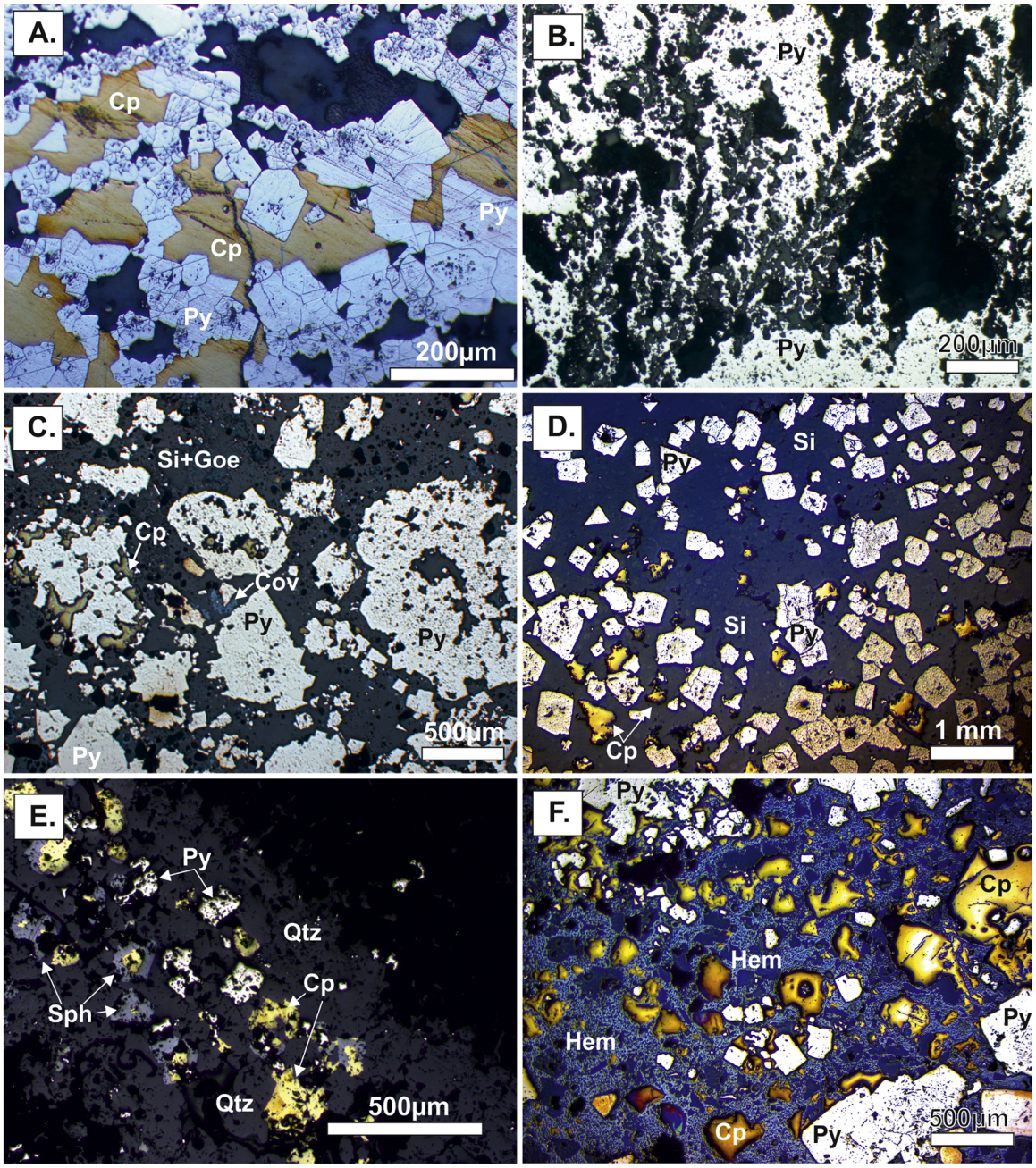

Fig. 4. Representative reflected light photomicrographs: (A) Massive pyrite and chalcopyrite, (B) dendritic pyrite, (C) granular-framboidal semi-massive pyrite, (D) semi-massive pyrite and chalcopyrite with goethite and silica, (E) stockwork mineralisation with pyrite, chalcopyrite and sphalerite, (F) South Apliki Breccia Zone mineralisation, hematite-pyrite-chalcopyrite. Cp = chalcopyrite, Py = pyrite, Sph = sphalerite, Cov = covellite, Hem = hematite, Qtz = quartz, Goe = goethite, Si = silica.

important in shallow recharge zones that occur distally to the high temperature VMS systems (e.g. Alt and Shanks, 2011; Pedersen et al., 2017; Rouxel et al., 2008). Hence, the majority of sulfur isotope data ($\delta^{34}S > 0‰$) in this study can be explained by mixing of sulfur leached from igneous host rocks (0-1‰; Alt, 1994) and the thermochemical reduction of Cretaceous seawater sulfate ($\delta^{34}S$ +18-19‰) in variable proportions at temperatures >160 °C.

Two models are proposed for the thermochemical reduction of seawater sulfate; the two-component mixing of seawater derived sulfate and igneous derived sulfide (Ono et al., 2007) and the anhydrite buffer model (Ohmoto et al., 1983). The two- component mixing of seawater sulfate ($\delta^{34}S \approx 21‰$, present day) and igneous derived sulfide ($\delta^{34}S \approx 0‰$, MORB) in active hydrothermal systems indicate that typically about >75% of H_2S is derived from leaching of igneous lithologies/sulfides with a minor seawater-derived sulfate component (<25%) (Ono et al., 2007). The anhydrite buffer model is based on the buffering of hydrothermal H_2S by anhydrite during fluid up flow (Ohmoto and Lasaga, 1982; Ohmoto et al., 1983). Equilibrium fractionation factors between sulfate and sulfide are temperature dependent, and fractionation factors range from 21.5‰ at 300 °C to 15.8‰ 400 °C (Ono et al., 2007; Ohmoto et al., 1983; Ohmoto and Lasaga, 1982). In contrast to the two-component mixing model the anhydrite buffer model predicts that a greater proportion of H_2S is sourced from the reduction of seawater sulfate (Ono et al., 2007).

These models are not mutually exclusive, for example at TAG, deep H_2S rich and SO_4 depleted (<1 mmol/kg) fluids undergo mixing with

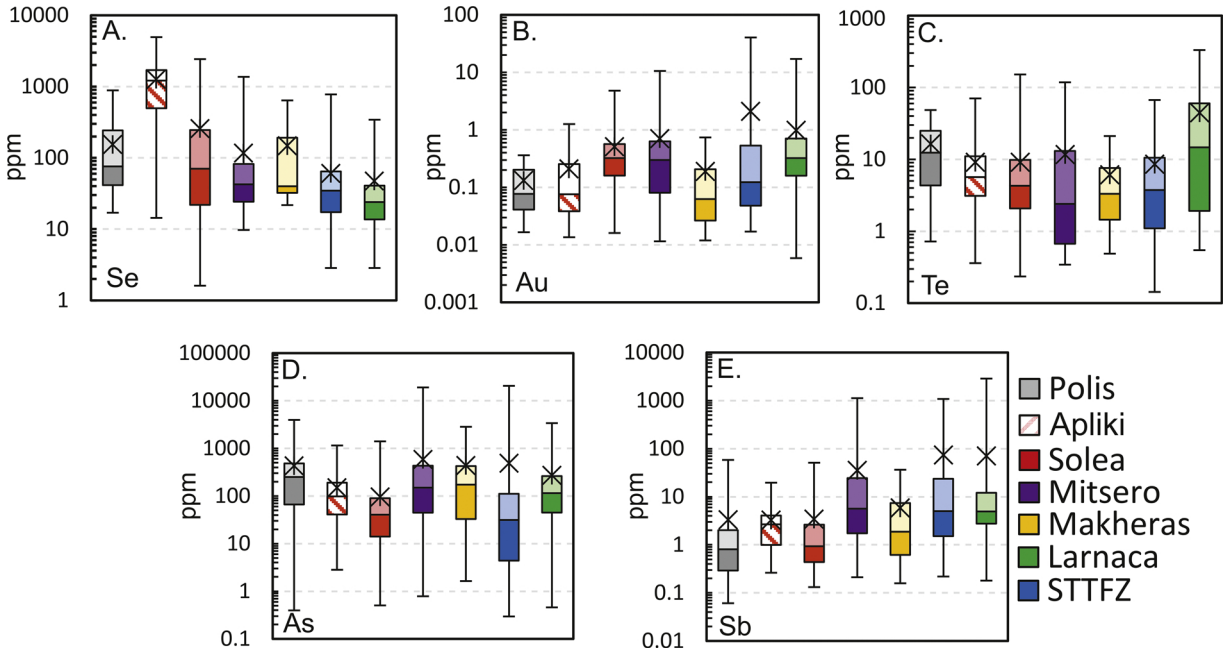

Fig. 5. Box plots of trace element concentrations in pyrite classified by structural domain (n = 1514, compiled data) (cf. Fig. 2): (A) Se, (B) Au, (C) Te, (D) As and (E) Sb. Apliki is presented separately due to its unusual enrichment in Se (See Martin et al., 2018). Light coloured box = lower quartile, dark coloured box = upper quartile, black line = median, black cross = average, error bars represent minimum and maximum values (Data compiled from: this study (n = 191), Keith et al., 2016a; Martin et al., 2018, 2019 (n = 1323)).

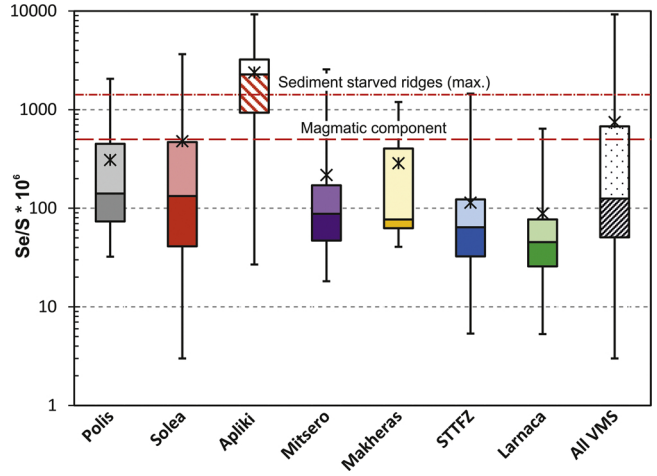

Fig. 6. Selenium/sulfur (Se/S× 10^6 vs. Se) ratios in pyrite (Total n = 1514, n = 191 this study) classified by structural domain (cf. Fig. 2). Selenium/sulfur ratios above the lower red dashed line suggest an increasing magmatic influx into the VMS hydrothermal system (>500). Upper dashed line marks the maximum Se/S ratio for modern sediment starved hydrothermal systems (1500; Layton-Matthews et al., 2008, 2013). Light coloured box = lower quartile, dark coloured box = upper quartile, black line = median, black cross = average, error bars represent minimum and maximum values (Data: This study (n = 191), Keith et al., 2016b; Martin et al., 2018, 2019). (For interpretation of the references to colour in this figure legend, the reader is referred to the web version of this article).

SO_4-rich fluids within the upflow zone (Humphris and Tivey, 2000). Anhydrite precipitation in the mixing zone is maintained by complex dissolution and re-precipitation processes and isotope exchange with deep H_2S rich fluids during mixing and entrainment of seawater at shallow crustal levels (Ono et al., 2007). If isotope equilibrium occurs during mixing, the composition of H_2S would plot along the anhydrite buffer line at the corresponding temperature (Ono et al., 2007). However, the coupled measurement of $\delta^{34}S$- $\delta^{18}O$ isotopes in anhydrite from

Table 5
Summary of sulfur isotope values in pyrite, chalcopyrite and covellite presented in per mil $\delta^{34}S_{(V\text{-}CDT)}$. Full data is available in Appendix A1.

PYRITE Deposit-δ34S (‰)	n =	σ	Average	Min.	Max.
Larnaca domain				**n = 55**	
Mathiatis North	40	1.3	5.1	2.5	7.2
Sha	9	2.4	1.5	−5.5	4.5
Touronja	2	0.6	1.9	1.3	2.4
Almyras	4	0.8	5.0	3.9	6.2
STTFZ				**n = 18**	
Kalavasos	18	4.3	8.0	2.0	13.2
Makheras				**5.0**	
Kampia	2	0.4	7.0	6.5	7.4
Kaphedes	2	1.7	5.0	3.3	6.6
Peristerka	1			5.4	5.4
Mitsero				**n = 20**	
Agrokipia A	3	0.6	4.8	4.1	5.6
Kokkinopezula	5	1.7	4.4	2.8	7.3
Kokkinoyia	8	3.5	3.2	−0.6	8.4
Akaki River	4	0.7	3.9	3.0	4.5
Solea				**n = 51**	
Apliki	19	1.7	4.2	−0.8	7.1
Memi	1			4.4	4.4
Skouriotissa	31	1.4	4.4	0.9	6.4
Polis				**n = 11**	
'77'	1			5.1	5.1
Kynousa	8	2.2	4.7	2.2	7.0
Lysos	1			7.1	7.1
Pournaji	1			9.5	9.5

CHALCOPYRITE Deposit- δ34S (‰)	n =	σ	Average	Min.	Max.
Kokkinoyia	1			0.6	0.6
Kokkinopezula	1			1.3	1.3
Apliki	11	0.9	3.6	2.4	5.2
Skouriotissa	2	0.7	4.9	4.2	5.6

COVELLITE Deposit- δ34S (‰)	n =	σ	Average	Min.	Max
Skouriotissa	5	0.7	4.5	3.7	5.3

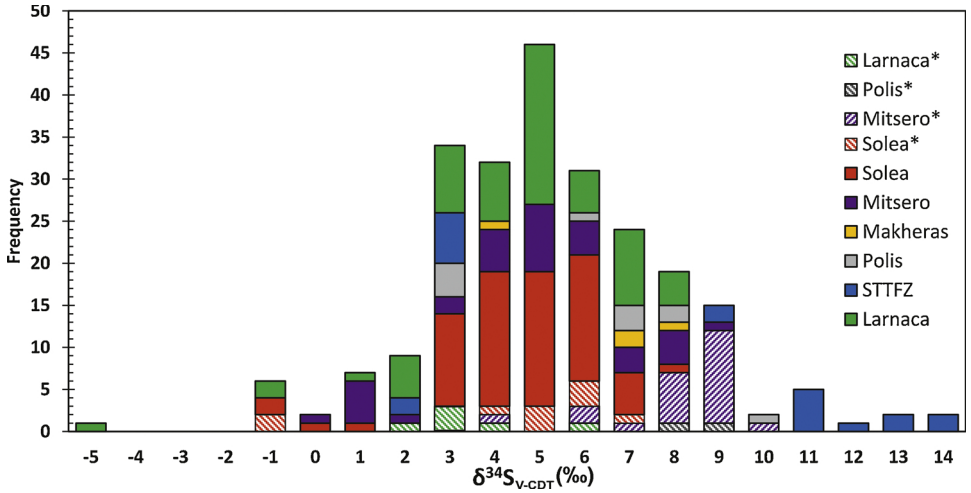

Fig. 7. Histogram of sulfur isotope ($\delta^{34}S$) compositions for all sulfides (n = 220: pyrite, chalcopyrite and covellite- Table 5) from investigated VMS deposits and other mineralised localities classified by their respective structural domains (cf. Fig. 2). *Dashed boxes refer to compiled data after Hannington et al. (1998), Keith et al. (2016a), Pedersen et al. (2017) (n = 40). Full data available in Appendix A1.

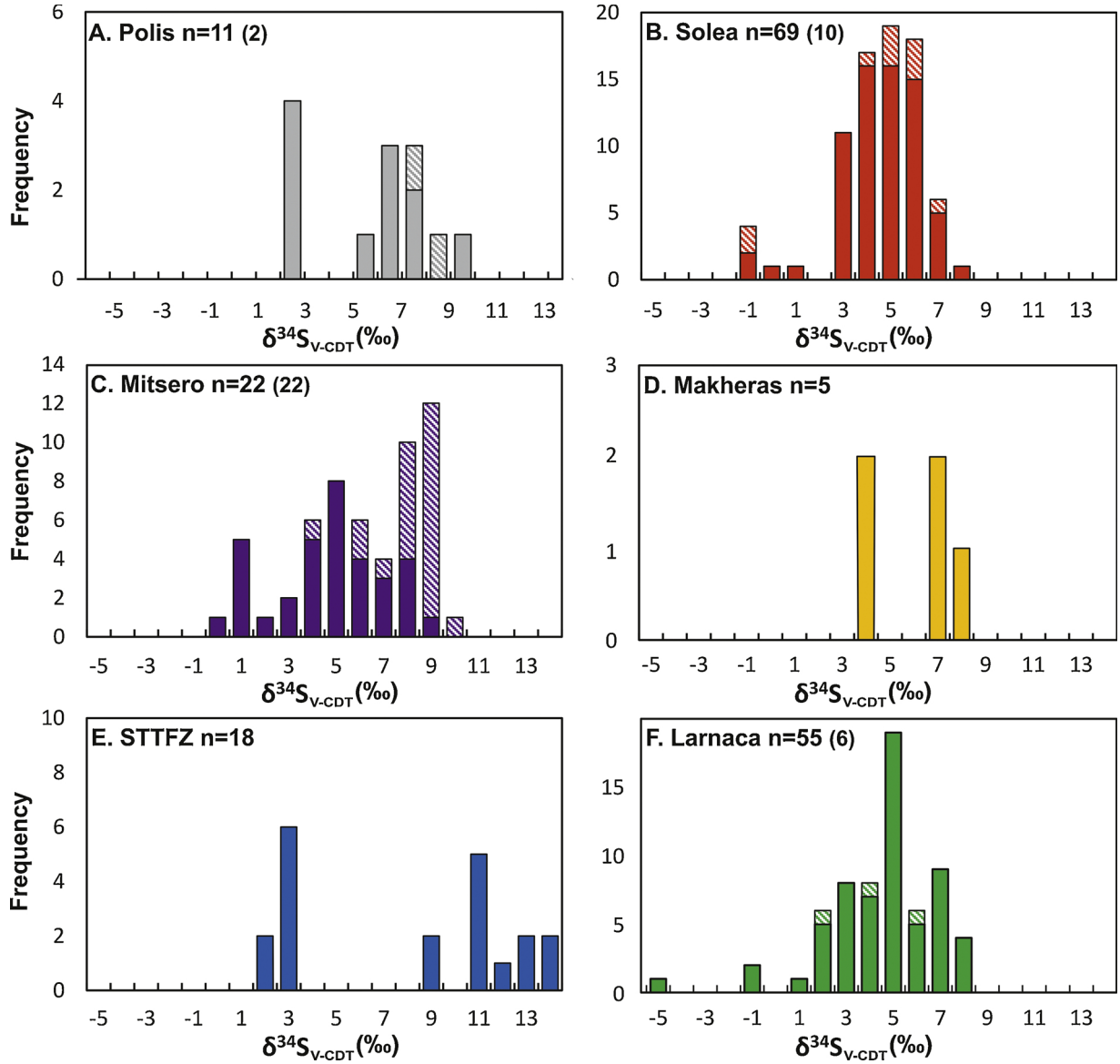

Fig. 8. Sulfur isotope $\delta^{34}S$ (‰ $_{V\text{-}CDT}$) data for all sulfides classified by structural domain (cf. Fig. 2). Dashed boxes refer to compiled data after Hannington et al. (1998), Keith et al. (2016a) and Pedersen et al. (2017). Number of analyses for each domain denoted by n, compiled values denoted by (n). Note variable Y axis values between different structural domains.

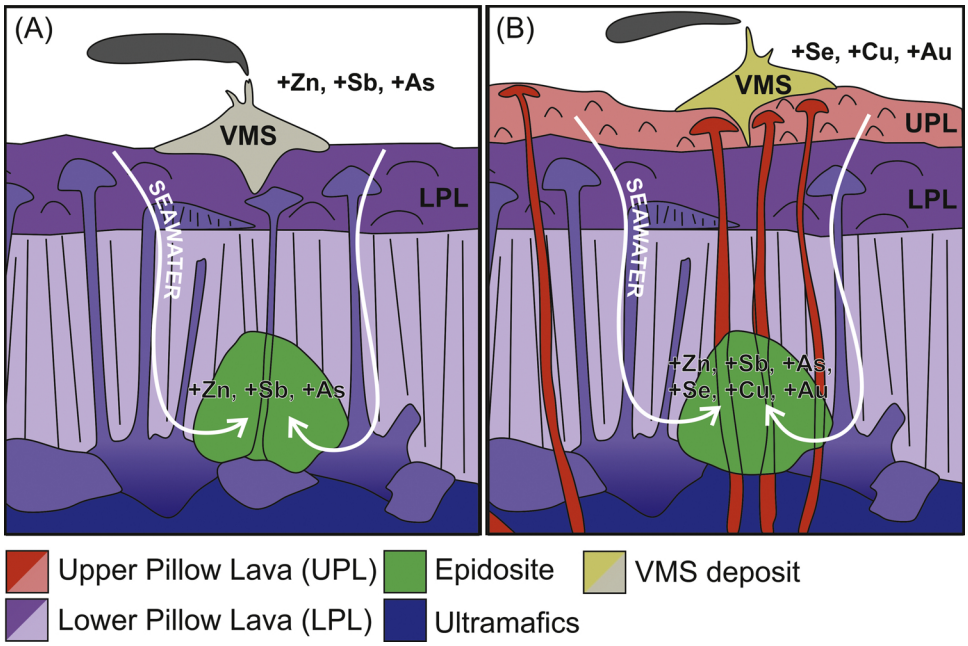

Fig. 9. Schematic model of the Troodos hydrothermal systems (not true to scale) showing the effect of source rock variation on VMS trace metal composition. (A) LPL source (purple) with VMS formation predating UPL accretion and, (B) VMS forming simultaneously or postdating UPL formation. VMS that formed through the alteration of Se, Cu and Au rich UPL are relatively enriched compared to those that predate UPL formation, forming exclusively from the leaching of LPL affinity dykes. The source of sulfur remains constant in both scenarios with $\delta^{34}S$ at or above the magmatic mean (0–1‰). (For interpretation of the references to colour in this figure legend, the reader is referred to the web version of this article).

Table 6
(A) Total 'UPL' (Au + Se + Cu) affinity elements vs. 'LPL' affinity elements (Zn + Sb + As) in ppm and average Se/S ratio with respect to the stratigraphic position of the different VMS deposits in the Troodos ophiolite, classified by structural domain (cf. Fig. 2). (B) Summary of all VMS deposits classified by stratigraphic depth.

(A)

Deposit	Au + Se + Cu (ppm)	Zn + Sb + As (ppm)	UPL:LPL	Stratigraphic level	Av. Se/S
Larnaca domain	n = 350				**89**
Mathiatis South	304	11561	0.03	UPL-LPL	71
Mathiatis North	482	1079	0.45	UPL-LPL	111
Sha	302	1158	0.26	UPL-LPL	63
STTFZ domain	n = 260				**114**
Kalavasos	121	955	0.13	UPL-LPL	114
Makheras domain	n = 40				**286**
Kampia	449	910	0.49	LPL	152
Kaphedes	920	2618	0.35	BG-LPL	454
Mitsero domain	n = 183				**217**
Agrokipia A	383	2352	0.16	UPL-LPL	56
Agrokipia B	307	21431	0.01	LPL	94
Kokkinopezula	199	185	1.08	LPL	164
Kokkinoyia	1599	7073	0.23	UPL-LPL	395
Solea domain	n = 362*				**481***
Apliki	3200	932	3.43	LPL	2381
Mala	2937	385	7.63	BG-LPL	168
Memi	207	20193	0.01	LPL	BDL
Skouriotissa	1381	1401	0.99	TOP OF UPL	500
Polis domain	n=137				**309**
'77'	28	915	0.03	LPL	52
Kynousa	1209	15718	0.08	TOP OF UPL	437
Limni	1423	7289	0.20	UPL	299
Pournaji	279	579	0.48	LPL	123

(B)

Stratigraphic depth	n (deposit)	Au + Se + Cu	As + Zn + Sb	UPL:LPL
Basal Group-LPL	2	920	2618	0.35
LPL/LPL-UPL contact	14	717	6284	0.25
Overlying UPL	2	1295	8559	0.53

the TAG mound indicate that sulfate was not in equilibrium with the hydrothermal fluid during precipitation (e.g., Chiba et al., 1998). This suggests a short fluid residence time and the incomplete exchange between SO_4 and H_2S resulting in fluids that plot around the two-phase mixing line (Ono et al., 2007). Further multiple sulfur isotope studies ($\Delta^{33}S$) would need to be undertaken to elucidate a single model.

Sulfur isotope values in pyrite from the Sha deposit (Larnaca domain) range from -5.5 to +4.5‰ and are the lowest values reported in this study (Fig. 7). Theoretically, these negative values could be explained by the anhydrite buffer model, assuming a fluid temperature of about 300 °C, fractionation of $\delta^{34}S$ between SO_4 and H_2S would be 21.5‰ (Ohmoto et al., 1983; Ono et al., 2007). If Cretaceous seawater had a $\delta^{34}S$ of 18-19‰, assuming equilibrium conditions, subsequent sulfides would have a corresponding $\delta^{34}S$ of between -3.5 to - 2.5‰, or

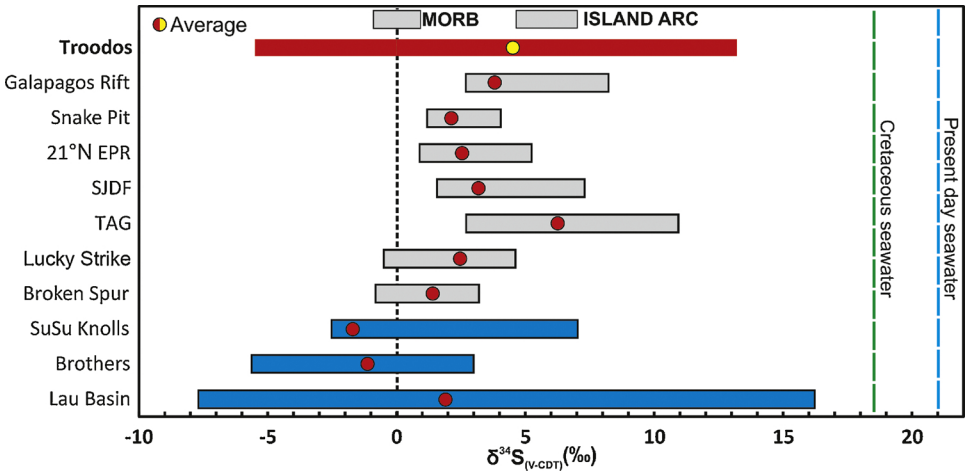

Fig. 10. Comparison of $\delta^{34}S$ of VMS deposits in Troodos (red bar) with active seafloor hydrothermal systems (pyrite, marcasite, sphalerite and chalcopyrite). Troodos (This study (n = 180), Hannington et al., 1998; Keith et al., 2016a; Pedersen et al., 2017), Galapagos Rift (Knott et al., 1995), Snake Pit (Kase et al., 1990), 21 °N East Pacific Rise (EPR) (Arnold and Sheppard, 1981; Woodruff and Shanks, 1988), Southern Juan de Fuca (SJDF) (Shanks and Seyfried, 1987), Trans- Atlantic Geotraverse Field (TAG) (Friedman, 1998; Gemmell and Sharpe, 1998; Herzig et al., 1998b), Lucky Strike (Rouxel et al., 2004), Broken Spur (Butler et al., 1998; Duckworth et al., 1995), SuSu Knolls (Yeats et al., 2014), Brothers (de Ronde et al., 2003d, 2005), Lau Basin (Herzig et al., 1998a). Red/yellow dots represent the average $\delta^{34}S$ value. Grey box represents the $\delta^{34}S$ composition of island arc lavas (Herzig et al., 1998a). Dashed lines: Black average MORB $\delta^{34}S$ composition, blue modern day seawater, green Cretaceous seawater (Kampschulte and Strauss, 2004). (For interpretation of the references to colour in this figure legend, the reader is referred to the web version of this article).

lighter if reactions took place at lower temperatures (Ono et al., 2007). As outlined previously and as demonstrated at TAG (Humphris and Tivey, 2000) and other SMS systems at the East Pacific Rise (Ono et al., 2007), a hybrid between the two-phase mixing and the anhydrite buffer model is preferred as fluids rarely reach equilibrium during their ascent to the seafloor.

Alternatively, light values similar to those observed in Troodos VMS are reported for sulfides in the Lau back-arc basin (Herzig et al., 1998a), at SuSu Knolls in the Manus back-arc basin (Yeats et al., 2014) and at the Brothers arc volcanic system (de Ronde et al., 2005d). The negative $\delta^{34}S$ values reported at modern vent sites are interpreted to be results of SO_2 disproportionation in a volatile phase. Exsolved SO_2 mixes with deep hydrothermal fluids causing disproportionation generating both H_2S and SO_4^{2-}; sulfides formed from this solution will have $\delta^{34}S$ <0‰ (Berkenbosch et al., 2012; de Ronde et al., 2005d). In combination, $\delta^{34}S$ and $Se/S \times 10^6$ ratios for Troodos VMS can be used as an indicator of magmatic volatile influx (Fig. 6, cf. section 5.5). Deposits that exhibit a $\delta^{34}S$ signature in sulfides <0‰ and contain elevated $Se/S \times 10^6$ >500 (e.g. Apliki or Skouriotissa) may have experienced an additional magmatic volatile influx. In contrast, the Se/S ratios of pyrite from the Larnaca domain that hosts the Sha deposit are mainly characterised by $Se/S \times 10^6$ <500 emphasising that the negative $\delta^{34}S$ values observed at Sha are likely due to the anhydrite buffer model or microbial sulfate reduction (Fig. 6).

Significant $\delta^{34}S$ variations of up to 11.2‰, from +2.0‰ to +13.2‰ are recorded in pyrite within the Kalavasos deposit (Table 5). In agreement with previous studies we relate this variability to the local channelling or reduced ingress of seawater with increasing depth in the VMS stratigraphy (i.e. stockwork vs. mound) leading to progressively lower $\delta^{34}S$ signatures. Similarly, at Skouriotissa we find $\delta^{34}S$ values in pyrite consistent with decreasing seawater ingress with stratigraphic depth ranging from +6.4‰ in the upper mound to +0.9‰ in the stockwork. This suggests that sulfide precipitation is influenced by complex physicochemical changes related to permeability, temperature and pH fluctuations (cm to m scale) along fluid flow pathways rather than a homogenous fluid flow throughout the mound (Martin et al., 2019).

When classified into regional structural domains (after Varga and Moores, 1985; Fig. 2) distinct $\delta^{34}S$ populations can be identified (Fig. 8). This is best illustrated within the STTFZ domain, where two distinct $\delta^{34}S$ populations in pyrite are identified at around +3‰ and +11‰ with an average of +8‰ (n = 18, Fig. 8E). The average $\delta^{34}S$ in pyrite for the STTFZ is notably higher than the Troodos VMS average (+4.6‰, all Troodos VMS, n = 160) suggesting larger volumes of seawater interaction. This is supported by the location of Kalavasos near the active transform terrain (Fig. 2). Isotopically heavy values in pyrite (up to +13.2‰ $\delta^{34}S$) are interpreted to have formed during the fault-controlled ingress of shallow circulating seawater that is only partially reduced in the shallow subsurface in addition to deeper circulating seawater derived fluids where sulfate is completely reduced to sulfide (e.g. Pedersen et al., 2017; a 'three stage mixing model'). In the three stage mixing model, sulfur is sourced through the thermochemical reduction of seawater sulfate, leaching of sulfur from igneous lithologies and the partial thermochemical reduction and entrainment of seawater at shallow crustal levels. In contrast, VMS deposits more distal to the transform fault experienced less shallow seawater interaction, leading to lighter but still positive $\delta^{34}S$ values in pyrite (Fig. 8, Table 5).

The relative contribution of sulfur sourced from seawater and leaching of igneous rocks assuming a two-phase mixing model has been calculated using the following equation:

$$\delta^{34}S_{mix} = X\ \delta^{34}S_{SW}\ (1\text{-}X)\ \delta^{34}S_0 \quad (1)$$

The sulfur isotope ratio of the fluid phase at each VMS deposit is represented by pyrite before ($\delta^{34}S_0$ = 0.5‰: Alt, 1994) and after mixing ($\delta^{34}S_{mix}$ = max. measured $\delta^{34}S$) with a certain amount of sulfur from Cretaceous seawater (X) ($\delta^{34}S_{SW}$ = 18.5‰: Kampschulte and Strauss, 2004).

The relative contribution of sulfur sourced from Cretaceous seawater was calculated for 19 mineralised localities (Table 5 and Fig. 11). Values for the Troodos VMS deposits range from 22% seawater derived sulfur at Sha to 71% at Kalavasos with an average for all deposits of 34% (Fig. 11). This is comparable to previous estimates by Keith et al. (2016a) for the Skouriotissa VMS deposit, where 38% of sulfur is derived from seawater. Consequently, depending on the individual VMS investigated, both the two-phase mixing model and the anhydrite buffer model may be applicable. This depends on the relative contribution of sulfur leached from igneous host rocks and the reduction of seawater sulfate, respectively. For example, at Sha only 22% of sulfur is derived from seawater thus favouring the two-phase mixing model; the opposite is true at Kalavasos where a greater proportion (71%) of sulfur is derived from seawater sulfate reduction.

5.5. Magmatic volatile influx

Constraints on the metal and sulfur source(s) in the crust are key to explain the magmatophile trace element variations (e.g., Te, Se, Au, Cu), Se/S ratios and $\delta^{34}S$ values in hydrothermal sulfides between structural domains and individual VMS deposits. We propose two

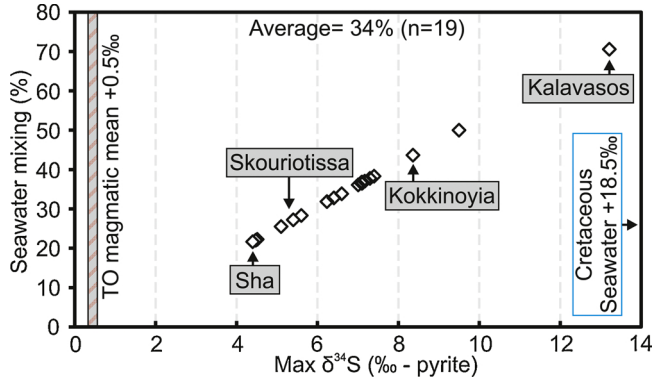

Fig. 11. Proportion of sulfur derived from seawater sulfate reduction vs. maximum $\delta^{34}S$ in pyrite (after Keith et al., 2016a). We assume a Troodos magmatic mean $\delta^{34}S$ value of +0.5‰ (Alt, 1994) and a value for Cretaceous seawater of +18.5‰ (Kampschulte and Strauss, 2004). Results demonstrate variable amounts of sulfur sourced from seawater with an average for all deposits (n = 19) of 34%.

principle processes: i) a heterogeneous source of metals within the lower sheeted dyke complex (Fig. 9, cf. section 5.2) and ii) a variable contribution of magmatic volatiles to the VMS hydrothermal systems (Fig. 12).

Variation in trace element geochemistry between different structural domains suggest a variable contribution of UPL and LPL affinity dykes within the source region of metals in the VMS systems (cf. section 5.2). However, $\delta^{34}S$ <0‰, i.e. less than the Troodos magmatic mean (0-1‰; Alt, 1994) and Se/S × 10^6 ratios >500 indicate a possible magmatic volatile contribution to the overlying VMS hydrothermal systems.

The exsolution and liberation of a magmatic volatile phase into the hydrothermal system during VMS formation can affect both $\delta^{34}S$ values and trace element concentrations of the precipitated sulfides (de Ronde et al., 2005d; Herzig et al., 1998a; Keith et al., 2018; Patten et al., 2019; Sillitoe et al., 1996; Yang and Scott, 2002). The Troodos lava chemistry is distinct compared to typical mid-ocean ridge basalts (MORB) and more comparable to melts generated in a subduction zone related setting (e.g. Lau back-arc) (Fonseca et al., 2017; Jenner et al., 2010; Miyashiro, 1973). This is in line with the elevated H_2O (2–6 wt.%; Fonseca et al., 2017), Au, As and Sb contents in the Troodos lavas relative to MORB and their more oxidising character (FMQ + 1.5) (Jenner et al., 2010; Patten et al., 2017). Upon reaching H_2O saturation, a magmatic volatile phase will likely exsolve from the residual melt, which may be contributed to an overlying hydrothermal system (Keith et al., 2018; Kelley and Robinson, 1990; Sun et al., 2004; Yang and Scott, 2002, 1996).

In the Troodos ophiolite magmas probably reached H_2O saturation; this is consistent with the elevated H_2O content of Troodos glass (2–6 wt.%; Fonseca et al., 2017). Ballhaus et al. (2015) report orbicular textures within gabbros of the Troodos lower plutonic sequence indicating H_2O saturation during cooling and crystallisation. Furthermore, fluid escape pathways are apparently preserved in the uppermost plutonics within plagiogranites (Ballhaus et al., 2015). These zones form sub-vertical veins and pods of massive epidote and albite. This probably indicates H_2O liberation from a solidifying hydrous magma body (Ballhaus et al., 2015). This evidence, in combination with the elevated H_2O content of the Troodos glass suggests that some Troodos magmas may have reached H_2O saturation.

Fluid inclusions from fresh and epidotised plagiogranites (Fig. 1) contain fluids of 46–56 wt.% NaCl equivalent with homogenisation temperatures between 400 and 500 °C (Cowan and Cann, 1988; Freund et al., 2014; Kelley et al., 2002, 1992; Kelley and Robinson, 1990). The pervasive occurrence of brines in the upper plutonics are explained by two processes; i) phase separation of seawater derived fluids and ii) the direct exsolution of volatiles from a silicate melt (Kelley et al., 1992). Kelley et al. (1992) showed that at a crustal depth of 3.5 km (550 bars pressure), fluids of seawater salinity would intersect the two-phase boundary at 500 °C, however fluids generated from this process would have salinities of 20–30 wt.% NaCl, notably less than those reported for plagiogranite hosted fluid inclusions.

Alternatively, volatiles could be directly exsolved from a silica saturated late stage melt in a low-pressure system (Kelley et al., 1992; Kelley and Robinson, 1990). Magmatic volatile-rich fluids have a

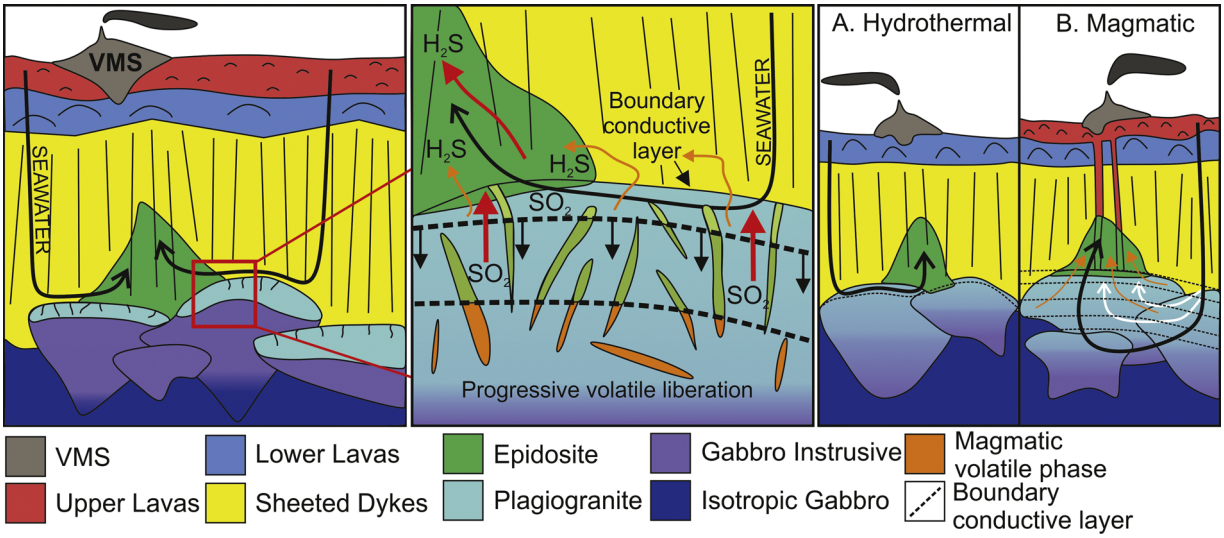

Fig. 12. Schematic model for volatile liberation at the Troodos magmatic-hydrothermal interface. Highly- saline fluid inclusions (>45 wt.% NaCl: Kelley and Robinson, 1990) provide evidence for volatile saturation. The progressive migration and fracturing of the boundary conductive layer due to crystallisation, repeated magma intrusion or overpressure caused by volatile saturation leads to the periodic migration of the boundary conductive layer to deeper levels (black dashed lines) and the release of magmatic volatile pulses carrying metals (orange and red arrows) into the overlying hydrothermal system in temporally distinct events. Periodic magmatic volatile release during magma intrusion and subsequent SO_2 disproportionation producing light H_2S that is incorporated in precipitated sulfides as $\delta^{34}S$ values <0‰ that are subsequently sporadically preserved in some Troodos VMS deposits. The two scenarios demonstrating an active (A) and immobile (B) boundary conductive layer are summarised by magmatic and hydrothermal schematic models. (For interpretation of the references to colour in this figure legend, the reader is referred to the web version of this article).

salinity of 1–7 wt.% NaCl upon initial exsolution from the melt, and, at high degrees of crystallisation, salinities can reach 80–90 wt.% NaCl. At higher pressures the salinity trend is reversed with maximum salinities reaching ~60 wt.% NaCl, comparable to those observed in fluid inclusions from the Troodos plagiogranites (Kelley et al., 1992).

The analysis of primary fluid inclusions in plutonic rocks show that with progressive melt fractionation, magmatic volatiles evolve from CO_2 – SO_2 rich vapours to immiscible CO_2 – H_2O rich vapours and finally metal −CO_2 – H_2O – NaCl brines (Kelley and Fruh-Green, 2000; Kelley et al., 2002); the latter is preserved in the Troodos plutonics. Pulsed volatile influx would cause the release of magmatically derived SO_2 vapour that undergoes disproportionation, forming H_2S and SO_4^{2-} (de Ronde et al., 2005d; Herzig et al., 1998a). Sulfides formed from this fluid will have a $\delta^{34}S$ signature of <0‰. A vapour phase is not readily preserved in the Troodos ophiolite but the preservation of 'end member' magmatic brines that form post-degassing suggest that SO_2 (and other volatiles in a vapour phase) were likely contributed to the hydrothermal system early in the magmatic evolution and prior to brine formation.

The addition of magmatic volatiles to the Troodos hydrothermal systems is preserved sporadically in the VMS mineralisation. Keith et al. (2016a) attributed negative $\delta^{34}S$ (-1.4‰) in pyrite from deep stockwork ores at Skouriotissa to a magmatic volatile influx. Here we present $\delta^{34}S$ values at Kokkinoyia (to -0.6‰, Mitsero domain) and Apliki (-0.8‰, Solea domain) that are also below the $\delta^{34}S$ composition of the primary lavas (0-1‰; Table 5 A, Fig. 8). The highest average $Se/S \times 10^6$ ratio, around the magmatic threshold (>500) was determined in pyrite from Skouriotissa at about 480 (max 3650) (Fig. 6) suggesting that the Skouriotissa hydrothermal system was affected by a magmatic volatile component. In contrast, the average $Se/S \times 10^6$ ratio of about 395 in pyrite from Kokkinoyia (Mitsero domain) is below the suggested magmatic threshold of 500 (Fig. 6), similarly at Sha low $Se/S \times 10^6$ that average 63 occur at low $\delta^{34}S$ (to −5.5‰). Hence, we propose that the negative $\delta^{34}S$ values that occur at low $Se/S \times 10^6$ ratios as observed at Kokkinoyia and Sha are likely the results of the low temperature seawater sulfate reduction under the anhydrite buffer model or perhaps microbial sulfate reduction. Both of which would shift $\delta^{34}S$ values in pyrite toward lighter values during sulfide precipitation independent of an additional magmatic volatile source. The limited preservation of sulfides with negative $\delta^{34}S$ values and $Se/S \times 10^6$ >500 could reflect the episodic nature of volatile release from the upper plutonics and the progressive overprinting of this volatile signature by subsequent seawater mixing (Gillis and Roberts, 1999; Keith et al., 2016a; Kelley et al., 2002; Kelley and Robinson, 1990).

Isotopic evidence ($^{87}Sr/^{86}Sr$, δO^{18}etc.) suggests that the boundary conductive layer between the sheeted dyke complex and plagiogranite bodies defines the lower limit of major hydrothermal convection (Bickle and Teagle, 1992; Gillis and Roberts, 1999; Richardson et al., 1987). As vapours are less dense than the surrounding fluid and would have been under significant pressure, they could easily migrate into the shallower hydrothermal systems. In contrast for denser brines, a liberation mechanism is required facilitating their transfer into the overlying ore-forming system (Fig. 12). The boundary conductive layer between the SDC and plutonics is mobile, fluctuating with the migrating crystallisation front, with changes in volatile exsolution pressure and the transition from ductile to brittle stress regimes (Kelley et al., 2002, 1992; Kelley and Robinson, 1990).

At Troodos, epidote veins occur within the uppermost plagiogranites indicating interaction with hydrothermal fluids (Gillis and Roberts, 1999; Richardson et al., 1987) (Fig. 12). The liberation of volatiles and associated brines would have been temporally distinct events but potentially important for the enrichment of trace elements and the contribution of SO_2-rich vapours and Cl^--rich brines to the hydrothermal systems and the associated VMS deposits. The Cl^-- rich and high temperature nature (400–500 °C) of brines could transport significant amounts of metals, leading to the enrichment of certain magmatophile elements in VMS deposits or districts (Brugger et al., 2007). The partitioning of metals between brine and vapour phase is variable and generally poorly constrained (e.g. Williams-Jones and Heinrich, 2005). Copper and Au have been suggested to preferentially partition into the vapour phase due to their enhanced complexation with sulfur species (Audétat et al., 2000, 1998; Williams-Jones and Heinrich, 2005). In contrast, Audétat and Pettke (2003) stated that the partitioning of Cu between vapour and brine is more complex and may vary between different magmatic-hydrothermal systems. Therefore, it remains enigmatic how metals in Troodos and other hydrothermal systems would partition between a vapour and brine phase liberated from an underlying magma body and contributed to an overlying hydrothermal system. However, it is clear that the liberation of either a volatile-rich brine or vapour phase into the overlying VMS hydrothermal systems would have a significant impact on the metal budget of the VMS deposits (e.g., Hedenquist and Lowenstern, 1994).

5.6. Implications for trace element distribution

Trace element geochemistry, Se/S ratios and sulfur isotope analyses highlight heterogeneities in the magmatic influx preserved in the Troodos VMS systems (Fig. 13). The data presented in this study suggests a combination of variable protolith compositions, the addition of a magmatic volatile phase followed by fluid seawater mixing and anhydrite buffering during fluid ascent controlling the metal and sulfur budget of the VMS systems. A significant portion of the sulfur isotope data between structural domains show positive $\delta^{34}S$ values (>0‰) (Figs. 7, 8 and 13) suggesting that the majority of sulfur in these systems is sourced through the leaching of igneous host rocks (av. = 66%) and the thermochemical reduction of seawater sulfate in varying quantities (22–75%; Fig. 11), probably favouring the two phase mixing model over the anhydrite buffer model. The source of sulfur within the SDC does not vary with trace element composition; primary magmatic $\delta^{34}S$ values between the UPL and LPL are indistinguishable (Alt, 1994; 0- 1‰). Therefore, the limited variation in $\delta^{34}S$ values in sulfides but variable trace element chemistry (Cu, Se, Au vs. Zn, Sb, As) and Se/S ratios between structural domains and individual VMS deposits can be explained by variable source rock compositions related to the relative proportion of UPL and LPL affinity dykes in the hydrothermal reaction zone.

The low $\delta^{34}S$ values in pyrite at Sha (to −5.5‰), Skouriotissa (to −1.4‰, Keith et al., 2016a), Apliki (to −0.8‰) and Kokkinoyia (to −0.6‰, Table 5) that are less than the Troodos magmatic mean (0–1‰; Alt, 1994) cannot only be explained through leaching of primary igneous lithologies. Whilst we propose that the light $\delta^{34}S$ values in Sha and Kokkinoyia is the result of anhydrite buffering or microbial sulfate reduction, we favour an additional metal and sulfur source for Apliki and Skouriotissa, most likely from the addition of a magmatic volatile phase (Fig. 13). The sporadic distribution of negative $\delta^{34}S$ values in pyrite suggests that these events were temporally and geographically discrete and/or are in many cases not preserved due to overprinting by later seawater dominated fluid pulses or seawater mixing, a phenomenon observed in modern immature SMS deposits (e.g., Hine Hina; Herzig et al., 1998a, Lucky Strike; Rouxel et al., 2004). Evidence exists in modern SMS deposits for pulsed magmatic activity, as observed in the CoAxial and North Cleft segment of the Juan de Fuca ridge (Butterfield et al., 1997; de Ronde et al., 2005d; Von Damm et al., 1997, 1985).

These results highlight the complexity of the Troodos ore-forming systems probably similar in scale to those observed at the Valu Fa Ridge in the Lau back-arc basin (Herzig et al., 1998a). On a regional scale, the SMS systems of the Valu Fa Ridge exhibit variations in $\delta^{34}S$ values from -5.3‰ (n = 9) to +11.7‰ (n = 4) at Hine Hina and Vai Lili; two hydrothermal systems located just ~40 km apart (Herzig et al., 1998a). Arguably, we see similar $\delta^{34}S$ variations in pyrite from the Troodos hydrothermal systems. For example, pyrite $\delta^{34}S$ from the Sha deposit

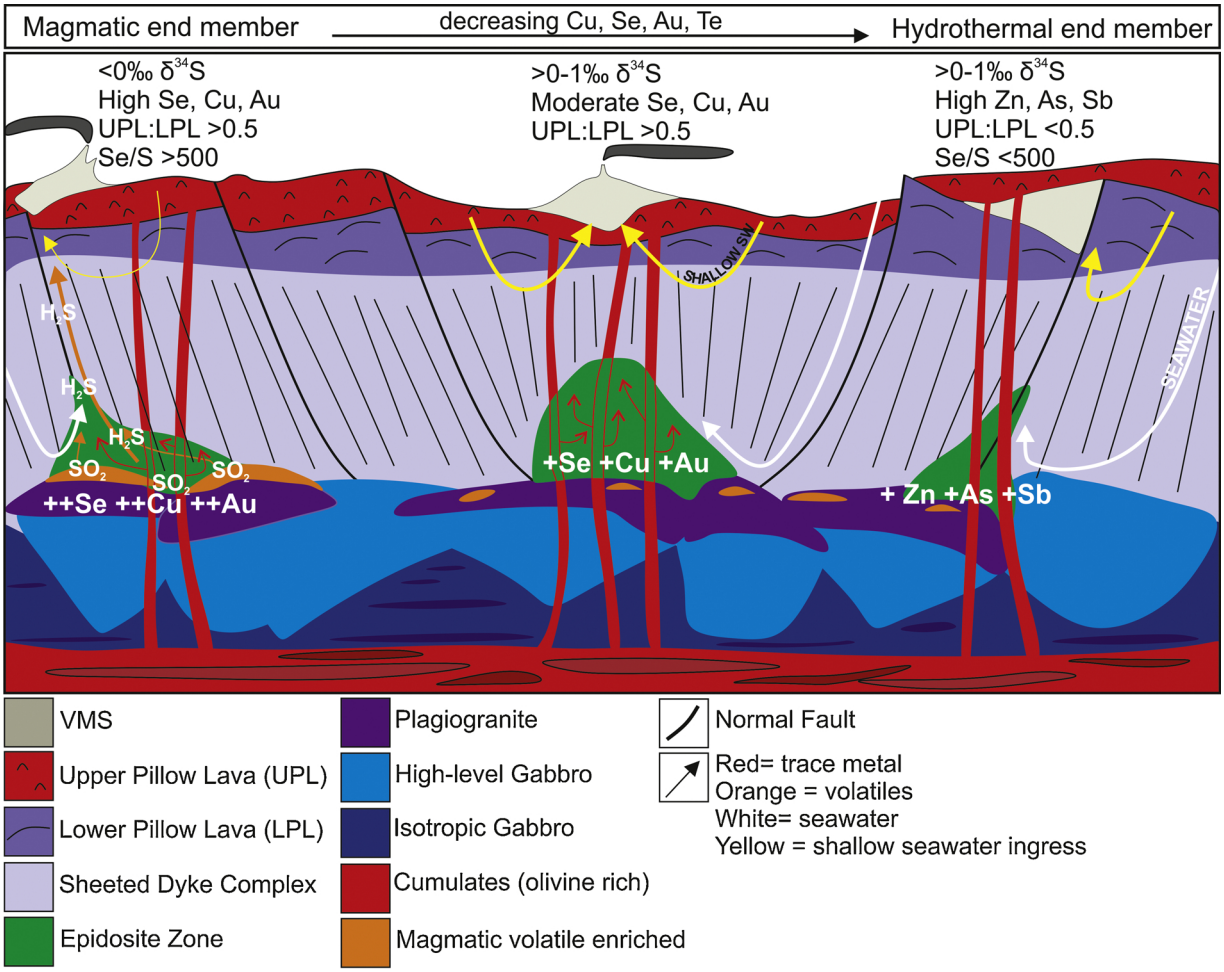

Fig. 13. Summary of VMS formation in the Troodos hydrothermal systems. Three scenarios explaining the transition from magmatic to hydrothermal end member VMS. (A) Both an UPL (Se, Cu, Au) source and magmatic volatile influx. VMS formed are enriched in Se, Cu, Au (and other magmatophile elements), exhibit a high UPL-LPL ratio and Se/S ratios >500 (Table 6A) and may exhibit negative $\delta^{34}S$ values. The yellow arrow indicates minor shallow seawater circulation. (B) Same as scenario A but with no evidence of magmatic volatile influx, or volatile influx has been subsequently overprinted by a seawater signature. Selenium, Cu and Au are enriched and UPL-LPL ratio remains elevated but $\delta^{34}S$ values <0‰ are absent. The shallow circulation of seawater is variable and denoted by yellow arrows. (C) Metals are sourced from a LPL source with minimal/no volatile influx. VMS are relatively enriched in Zn, As and Sb and exhibit a low UPL-LPL ratio and low Se/S < 500. $\delta^{34}S$ values are the same as B; at or above the Troodos magmatic mean (0–1‰). (For interpretation of the references to colour in this figure legend, the reader is referred to the web version of this article).

reaches values as low as -5.5‰, while pyrite from Kalavasos reach $\delta^{34}S$ values of up to +13.2‰, these deposits are located only 20 km apart. Consequently, two endmember systems can be defined for the Troodos VMS deposits including; i) magmatic dominated systems characterised by $\delta^{34}S$ <0‰, elevated Se/S × 10^6 >500 and high Se, Cu and Au, as well as ii) hydrothermal dominated systems with $\delta^{34}S$ >0‰, Se/S × 10^6 <500 and high Zn, As and Sb (Fig. 13).

6. Summary and conclusion

The regional application of trace element geochemistry, Se/S ratios and sulfur isotopes reveals a variable metal source in the hydrothermal systems and associated VMS deposits of the Troodos ophiolite, Cyprus. This relates to i) a variable trace element chemistry of the sheeted dykes in the source region and ii) the addition of a metal-bearing magmatic volatile phase to some hydrothermal systems. We apply an updated regional scale ore-forming model that explains the distribution and enrichment of magmatophile trace elements and $\delta^{34}S$ values in hydrothermal sulfides across the Troodos ophiolite. Sheeted dykes with a trace element chemistry resembling the depleted UPL contain elevated Se, Cu and Au relative to the non-depleted LPL suite. The relative proportion of these two suites controls the enrichment of Cu, Se and Au relative to As, Zn and Sb in the overlying VMS deposits.

The light $\delta^{34}S$ values (<0‰) preserved in some VMS deposits are interpreted to be either the result of anhydrite buffering during fluid upflow, the microbial mediated low temperature (<120 °C) reduction of seawater sulfate (Sha, Kokkinoyia, Se/S × 10^6 <500) or a magmatic volatile component contributed to the hydrothermal system (Apliki, Skouriotissa, Se/S × 10^6 >500). In order to confirm these results, multiple sulfur isotope analyses ($\Delta^{33}S$) would need to be undertaken.

The addition of magmatic volatiles to the hydrothermal system probably relates to the liberation of a volatile phase (e.g., SO_2) that formed through exsolution directly from a volatile saturated melt during melt intrusion or the migration of the boundary conductive layer to deeper crustal levels. The liberation of volatiles were temporally and geographically discrete events. The subsequent disproportionation of magmatic SO_2 in the deeper hydrothermal system is preserved as discrete negative $\delta^{34}S$ values combined with Se/S × 10^6 ratios >500 in pyrite. The trace element data and sulfur isotope signature of the Troodos hydrothermal systems and its associated VMS deposits are consistent with our current understanding that Troodos formed in the vicinity of a subduction zone and that the processes responsible for VMS formation differ from those at mid-ocean ridge settings.

We can confirm that this work has not been published previously

and is not under consideration for publication in any other journal. A.J. Martin wrote the initial manuscript. A.J. Martin, M. Keith and D.B. Parvaz were all involved in the collection of sulfur isotope data. A.J. Boyce supervised the collection of sulfur isotope data for dataset A (SUERC) and H. Strauss dataset B (Münster). I. McDonald supervised the collection of LA-ICP-MS trace element data at Cardiff University. C.J MacLeod, G.R.T Jenkin and K.A McFall were involved in discussion and editing of the manuscript. All authors approve the publication of this manuscript in *Chemical Geology*.

Declaration of Competing Interest

We can confirm that this work has not been published previously and is not under consideration for publication in any other journal. A.J. Martin wrote the initial manuscript. A.J. Martin, M. Keith and D.B. Parvaz were all involved in the collection of sulfur isotope data. A.J. Boyce supervised the collection of sulfur isotope data for dataset A (SUERC) and H. Strauss dataset B (Münster). I. McDonald supervised the collection of LA-ICP-MS trace element data at Cardiff University. C.J MacLeod, G.R.T Jenkin and K.A McFall were involved in discussion and editing of the manuscript. All authors approve the publication of this manuscript in *Chemical Geology*.

Acknowledgments

This research was supported by the Natural Environmental Research Council (NERC) under the tellurium and selenium cycling and supply (TeaSe) grant NE/M010848/1. Isotope analyses was supported by the NERC Isotope Geosciences Facilities Steering Committee grants IP-1766-1117 (Martin) and IP-1261-0511 (Parvaz). We kindly thank Alison McDonald for her assistance during isotope analysis. Dr. Andreas Zissimos and the Director of the Geological Survey Department Dr. Costas Constantinou are thanked for their continued support and enthusiasm towards this project. We also thank Hellenic Copper Mines, Dr. Michael Green, Ifigenia Gavriel and Lazaros Georgiou for discussion and their assistance in the field. We thank Prof. Jeffery Alt and an anonymous reviewer for their comments that improved the quality of this manuscript. We also thank Dr. Catherine Chauvel for the efficient editorial handling of the manuscript.

Appendix A. Supplementary data

Supplementary material related to this article can be found, in the online version, at doi:https://doi.org/10.1016/j.chemgeo.2019.119325.

References

Adamides, N., 2010. Mafic-dominated volcanogenic sulphide deposits in the Troodos ophiolite, Cyprus Part 2- a review of genetic models and guides for exploration. Appl. Earth Sci. 119, 193–204.
Allerton, S., Vine, F., 1991. Spreading evolution of the Troodos ophiolite, Cyprus. Geology 19, 637–640.
Alt, J.C., 1994. A sulfur isotopic profile through the Troodos ophiolite, Cyprus: primary composition and the effects of seawater hydrothermal alteration. Geochim. Cosmochim. Acta 58, 1825–1840.
Alt, J.C., Teagle, D.A., Brewer, T., Shanks III, W.C., Halliday, A., 1998. Alteration and mineralization of an oceanic forearc and the ophiolite-ocean crust analogy. J. Geophys. Res. Solid Earth 103 (B6), 12365–12380.
Alt, J.C., Shanks, W.C., 2011. Microbial sulfate reduction and the sulfur budget for a complete section of altered oceanic basalts, IODP Hole 1256D (eastern Pacific). Earth Planet. Sci. Lett. 310 (1-2), 73–83.
Arnold, M., Sheppard, S.M.F., 1981. East Pacific rise at latitude 21°N: isotopic composition and origin of the hydrothermal sulphur. Earth Planet. Sci. Lett. 56, 148–156.
Audétat, A., Günther, D., Heinrich, C.A., 2000. Causes for large- scale metal zonation around mineralized plutons: fluid inclusion LA-ICP-MS evidence from the Mole Granite, Australia. Econ. Geol. 95, 1563–1581.
Audétat, A., Günther, D., Heinrich, C.A., 1998. Formation of a magmatic-hydrothermal ore deposit: insights with LA- ICP-MS analysis of fluid inclusions. Science 279, 2091–2094.
Audétat, A., Pettke, T., 2003. The magmatic-hydrothermal evolution of two barren granites: a melt and fluid inclusion study of the Rito del Medio and Canada Pinabete plutons in northern New Mexico (USA). Geochim. Cosmochim. Acta 67, 97–121.
Ballhaus, C., Fonseca, R.O.C., Münker, C., Kirchenbaur, M., Zirner, A., 2015. Spheroidal textures in igneous rocks – textural consequences of H_2O saturation in basaltic melts. Geochim. Cosmochim. Acta 167, 241–252.
Baragar, W.R., Lambert, N., Baglow, N., Gibson, I., 1990. The sheeted dyke zone in the Troodos ophiolite. OPHIOLITES Oceanic Crustal Analogues, Proceedings of the Symposium "Troodos 1987" The Geological Survey Department, Ministry of Agriculture and Natural Resources, Nicosia, Cyprus, pp. 37–51.
Berkenbosch, H.A., Ronde, C.E.J. de, Gemmell, J.B., McNeill, A.W., Goemann, K., 2012. Mineralogy and formation of black smoker chimneys from brothers submarine volcano. Kermadec Arc. Econ. Geol. 107, 1613–1633.
Bickle, M.J., Teagle, D.A.H., 1992. Strontium alteration in the Troodos ophiolite: implications for fluid fluxes and geochemical transport in mid- ocean ridge hydrothermal systems. Earth Planet. Sci. Lett. 113, 219–237.
Brugger, J., Etschmann, B., Liu, W., Testemale, D., Hazemann, J.L., Emerich, H., van Beek, W., Proux, O., 2007. An XAS study of the structure and thermodynamics of Cu (I) chloride complexes in brines up to high temperature (400 °C, 600 bar). Geochim. Cosmochim. Acta 71, 4920–4941.
Butler, I.B., Fallick, A.E., Nesbitt, R.W., 1998. Mineralogy, sulphur isotope geochemistry and the development of sulphide structures at the Broken Spur hydrothermal vent site, 29°10'N, Mid-Atlantic Ridge. J. Geol. Soc. 155, 773–785.
Butterfield, D.A., Massoth, G.J., McDuff, R.E., Lupton, J.E., Lilley, M.D., 1990. Geochemistry of hydrothermal fluids from Axial Seamount hydrothermal emissions study vent field, Juan de Fuca Ridge: subseafloor boiling and subsequent fluid-rock interaction. J. Geophys. Res. Solid Earth 95, 12895–12921.
Butterfield, D.A., Jonasson, I.R., Massoth, G.J., Feely, R.A., Roe, K.K., Embley, R.E., Holden, J.F., McDuff, R.E., Lilley, M.D., Delaney, J.R., 1997. Seafloor eruptions and evolution of hydrothermal fluid chemistry. Phil. Trans. R. Soc. Lond. Ser. A 355 (1723), 369–386.
Chiba, H., Uchiyama, N., Teagle, D.A., 1998. Stable isotope study of anhydrite and sulfide minerals at the TAG hydrothermal mound, Mid-Atlantic Ridge, 26 N. In: Proceedings-Ocean Drilling Program Scientific Results. NSF. pp. 85–90.
Constantinou, G., 1980. Metalogenesis associated with Troodos ophiolite. In: Ophiolites, Proceedings: International Ophiolite Synposium, Cyprus 1979. The Geological Survey Department, Ministry of Agriculture and Natural Resources, Nicosia, Cyprus. pp. 663–674.
Constantinou, G., Govett, G.J.S., 1973. Geology, geochemistry, and genesis of Cyprus sulfide deposits. Econ. Geol. 68, 843–858.
Cowan, J., Cann, J., 1988. Supercritical two-phase separation of hydrothermal fluids in the Troodos ophiolite. Nature 333, 259–261.
de Ronde, C.E., Faure, K., Bray, C.J., Chappell, D.A., Wright, I.C., 2003d. Hydrothermal fluids associated with seafloor mineralization at two southern Kermadec arc volcanoes, offshore New Zealand. Miner. Deposita 38, 217–233.
de Ronde, C.E.J., Hannington, M.D., Stoffers, P., Wright, I.C., Ditchburn, R.G., Reyes, A.G., Baker, E.T., Massoth, G.J., Lupton, J.E., Walker, S.L., Greene, R.R., Soong, C.W.R., Ishibashi, J., Lebon, G.T., Bray, C.J., Resing, J.A., 2005d. Evolution of a submarine magmatic-hydrothermal system: brothers volcano, southern Kermadec Arc, New Zealand. Econ. Geol. 100, 1097–1133.
Duckworth, R.C., Knott, R., Fallick, A.E., Rickard, D., Murton, B.J., Dover, C.V., 1995. Mineralogy and sulphur isotope geochemistry of the Broken spur sulphides, 29°N, Mid-Atlantic Ridge. Geol. Soc. Lond. Spec. Publ. 87, 175–189.
Everdingen, D.A. van, Cawood, P.A., Everdingen, D.A. van, Cawood, P.A., 1995. Dyke domains in the Mitsero graben, Troodos ophiolite, Cyprus: an off-axis model for graben formation at a spreading centre. J. Geol. Soc. 152, 923–932.
Franklin, J.M., Gibson, H.L., Jonasson, I.R., Galley, A.G., 2005. Volcanogenic massive Sule deposits. Econ. Geol. 100, 523–560.
Fonseca, R.O.C., Kirchenbaur, M., Ballhaus, C., Münker, C., Zirner, A., Gerdes, A., Heuser, A., Botcharnikov, R., Lenting, C., 2017. Fingerprinting fluid sources in Troodos ophiolite complex orbicular glasses using high spatial resolution isotope and trace element geochemistry. Geochim. Cosmochim. Acta 200, 145–166.
Fouquet, Y., Stackelberg, Uvon, Charlou, J.L., Erzinger, J., Herzig, P.M., Muehe, R., Wiedicke, M., 1993. Metallogenesis in back-arc environments; the Lau Basin example. Econ. Geol. 88, 2154–2181.
Friedman, C.T., 1998. Analysis of stable sulfur isotopes and trace cobalt on sulfides from the TAG hydrothermal mound. Doctoral dissertation. Massachusetts Institute of Technology.
Freund, S., Haase, K.M., Keith, M., Beier, C., Garbe-Schönberg, D., 2014. Constraints on the formation of geochemically variable plagiogranite intrusions in the Troodos Ophiolite, Cyprus. Contrib. Mineral. Petrol. 167, 978.
Gass, I.G., 1980. The Troods massif: its role in the unravelling of the ophiolite problem and its significance in the understanding of constructive plate margin processes. In: Ophiolites, Proceedings: International Ophiolite Synposium, Cyprus 1979. The Geological Survey Department, Ministry of Agriculture and Natural Resources, Nicosia, Cyprus. pp. 23–35.
German, C.R., Von Damm, K.L., 2004. Hydrothermal processes. In: Holland, H.D., Turekian, K.K. (Eds.), Treatise On Geochemistry, vol. 6, The Oceans and Marine Geochemistry. Elsevier, London, pp. 181–222.
Gillis, K.M., Roberts, M.D., 1999. Cracking at the magma–hydrothermal transition: evidence from the Troodos Ophiolite, Cyprus. Earth Planet. Sci. Lett. 169, 227–244.
Gemmell, J.B., Sharpe, R., 1998. Detailed sulfur-isotope investigation of the TAG hydrothermal mound and stockwork zone, 26 N, Mid-Atlantic Ridge. In: Proceedings-Ocean Drilling Program Scientific Results. National Science Foundation. pp. 71–84.
Grant, H.L.J., Hannington, M.D., Petersen, S., Frische, M., Fuchs, S.H., 2018. Constraints on the behavior of trace elements in the actively-forming TAG deposit, Mid-Atlantic Ridge, based on LA-ICP-MS analyses of pyrite. Chem. Geol. 498, 45–71.

Hannington, M., Jamieson, J., Monecke, T., Petersen, S., Beaulieu, S., 2011. The abundance of seafloor massive sulfide deposits. Geol. Soc. Am.
Hannington, M.D., Barrie, C.T., Bleeker, W., 1999. The Giant Kidd Creek volcanogenic massive sulfide deposit, Western Abitibi Subprovince, Canada: summary and synthesis. In: Hannington, M.D., Barrie, C.T. (Eds.), The Giant Kidd Creek Volcanogenic Massive Sulfide Deposit. Canada Society of Economic Geologists, Western Abitibi Subprovince.
Hannington, M.D., Galley, A., Gerzig, P., Petersen, S., 1998. Comparison of the TAG mound and stockwork complex with Cyprus- type massive sulfide deposits. Proc. Ocean Drill. Prog. Sci. Results 158, 389–415.
Hedenquist, J.W., Lowenstern, J.B., 1994. The role of magmas in the formation of hydrothermal ore deposits. Nature 370 (6490), 519.
Herzig, P.M., Hannington, M.D., Jr, A.A., 1998a. Sulfur isotopic composition of hydrothermal precipitates from the Lau back-arc: implications for magmatic contributions to seafloor hydrothermal systems. Miner. Deposita 33, 226–237.
Herzig, P.M., Petersen, S., Hannington, M.D., 1998b. Geochemistry and sulfur-isotopic composition of the TAG hydrothermal mound, Mid-Atlantic Ridge, 26 N. In: Proceedings-Ocean Drilling Program Scientific Results. National Science Foundation. pp. 47–70.
Humphris, S.E., Herzig, P.M., Miller, D.J., Alt, J.C., Becker, K., Brown, D., Brügmann, G., Chiba, H., Fouquet, Y., Gemmell, J.B., Guerin, G., Hannington, M.D., Holm, N.G., Honnorez, J.J., Iturrino, G.J., Knott, R., Ludwig, R., Nakamura, K., Petersen, S., Reysenbach, A.-L., Rona, P.A., Smith, S., Sturz, A.A., Tivey, M.K., Zhao, X., 1995. The internal structure of an active sea-floor massive sulphide deposit. Nature 377, 713–716.
Humphris, S.E., Klein, F., 2018. Progress in deciphering the controls on the geochemistry of fluids in seafloor hydrothermal systems. Annu. Rev. Mar. Sci. 10, 315–343.
Humphris, S.E., Tivey, M.K., 2000. A synthesis of geological and geochemical investigations of the TAG hydrothermal fluid: Insights into fluid flow and mixing processes in a hydrothermal system. In: In: Dilek, Y., Moores, E., Elthon, D., Nicolas, A. (Eds.), Ophiolites and Oceanic Crust: New Insights from Field Studies and the Ocean Drilling Program 349. Geol. Soc. of Am. Special Paper, Boulder, CO, pp. 213–235.
Hurst, S.D., Moores, E.M., Varga, R.J., 1994. Structural and geophysical expression of the Solea graben, Troodos Ophiolite, Cyprus. Tectonics 13, 139–156.
Huston, D.L., Sie, S.H., Suter, G.F., 1995. Selenium and its importance to the study of ore genesis: the theoretical basis and its application to volcanic-hosted massive sulfide deposits using pixeprobe analysis. Nucl. Instrum. Methods Phys. Res. Sect. B 104, 476–480.
Jenner, F.E., O'Neill, H.S.C., Arculus, R.J., Mavrogenes, J.A., 2010. The Magnetite crisis in the evolution of arc-related magmas and the initial concentration of Au, Ag and Cu. J. Petrol. 51.
Jowitt, S.M., Jenkin, G.R.T., Coogan, L.A., Naden, J., 2012. Quantifying the release of base metals from source rocks for volcanogenic massive sulfide deposits: effects of protolith composition and alteration mineralogy. J. Geochem. Explor. 118, 47–59.
Kampschulte, A., Strauss, H., 2004. The sulfur isotopic evolution of Phanerozoic seawater based on the analysis of structurally substituted sulfate in carbonates. Chem. Geol. 204, 255–286.
Kase, K., Yamamoto, M., Shibata, T., 1990. Copper-rich sulfide deposit near 23 N, Mid-Atlantic Ridge: chemical composition, mineral chemistry, and sulfur isotopes. Proc., scientific results, ODP, Legs 106/109, Mid-Atlantic Ridge 163–177.
Keith, M., Haase, K.M., Klemd, R., Krumm, S., Strauss, H., 2016a. Systematic variations of trace element and sulfur isotope compositions in pyrite with stratigraphic depth in the Skouriotissa volcanic- hosted massive sulfide deposit, Troodos ophiolite, Cyprus. Chem. Geol.
Keith, M., Häckel, F., Haase, K.M., Schwarz- Schampera, U., Klemd, R., 2016b. Trace element systematics of pyrite from submarine hydrothermal vents. Ore Geol. Rev. 72, 728–745.
Keith, M., Haase, K.M., Klemd, R., Smith, D.J., Schwarz- Schampera, U., Bach, W., 2018. Constraints on the source of Cu in a submarine magmatic- hydrothermal system, Brothers volcano, Kermadec island arc. Contrib. Mineral. Petrol. 173 (40), 1–16.
Kelley, D.S., Baross, J.A., Delaney, J.R., 2002. Volcanoes, fluids, and life at mid-ocean ridge spreading centers. Annu. Rev. Earth Planet. Sci. 30, 385–491.
Kelley, D.S., Fruh-Green, G.L., 2000. Volatiles in Mid- Ocean Ridge Environments. Special Papers-Geol. Soc. of America. pp. 237–260.
Kelley, D.S., Robinson, P.T., 1990. Development of a brine-dominated hydrothermal system at temperatures of 400–500°C in the upper level plutonic sequence, Troodos ophiolite, Cyprus. Geochim. Cosmochim. Acta 54, 653–661. https://doi.org/10.1016/0016-7037(90)90361-N.
Kelley, D.S., Robinson, P.T., Malpas, J.G., 1992. Processes of brine generation and circulation in the oceanic crust: Fluid inclusion evidence from the Troodos Ophiolite, Cyprus. J. Geophys. Res. Solid Earth 97, 9307–9322.
Knott, R., Fallick, A.E., Rickard, D., Bäcker, H., 1995. Mineralogy and sulphur isotope characteristics of a massive sulphide boulder, Galapagos Rift, 85°55′W. Geol. Soc. Lond. Spec. Publ. 87, 207–222.
Koschinsky, A., Garbe- Schönberg, D., Sander, S., Schmidt, K., Gennerich, H.-H., Strauss, H., 2008. Hydrothermal venting at pressure-temperature conditions above the critical point of seawater, 5°S on the Mid-Atlantic Ridge. Geology 36, 615–618.
Layton- Matthews, D., Leybourne, M.I., Peter, J.M., Scott, S.D., Cousens, B., Eglington, B.M., 2013. Multiple sources of selenium in ancient seafloor hydrothermal systems: Compositional and Se, S, and Pb isotopic evidence from volcanic-hosted and volcanic-sediment-hosted massive sulfide deposits of the Finlayson Lake District, Yukon, Canada. Geochim. Cosmochim. Acta 117, 313–331.
Layton- Matthews, D., Peter, J.M., Scott, S.D., Leybourne, M.I., 2008. Distribution, Mineralogy, and Geochemistry of Selenium in Felsic Volcanic-Hosted Massive Sulfide Deposits of the Finlayson Lake District, Yukon Territory, Canada. Econ. Geol. 103, 61–88.
Little, C.T.S., Cann, J.R., Herrington, R.J., Morisseau, M., 1999. Late Cretaceous hydrothermal vent communities from the Troodos ophiolite, Cyprus. Geology 27, 1027–1030.
Machel, H.G., 2001. Bacterial and thermochemical sulfate reduction in diagenetic settings—old and new insights. Sed. Geol. 140 (1-2), 143–175.
Malpas, J., Langdon, G., 1984. Petrology of the Upper Pillow Lava suite, Troodos ophiolite, Cyprus. Geol. Soc. Lond. Spec. Publ. 13, 155–167.
Martin, A.J., Keith, M., McDonald, I., Haase, K.M., McFall, K.A., Klemd, R., MacLeod, C.J., 2019. Trace element systematics and ore-forming processes in mafic VMS deposits: Evidence from the Troodos ophiolite, Cyprus. Ore Geol. Rev. 106, 205–225.
Martin, A.J., McDonald, I., MacLeod, C.J., Prichard, H.M., McFall, K., 2018. Extreme enrichment of selenium in the Apliki Cyprus-type VMS deposit, Troodos. Cyprus. Mineral. Mag. 82, 697–724.
Maslennikov, V.V., Maslennikova, S.P., Large, R.R., Danyushevsky, L.V., 2009. Study of trace element zonation in vent chimneys from the Silurian Yaman-Kasy volcanic-hosted massive sulfide deposit (Southern Urals, Russia) using laser ablation-inductively coupled plasma mass spectrometry (LA-ICPMS). Econ. Geol. 104, 1111–1141.
McDermott, J.M., Ono, S., Tivey, M.K., Seewald, J.S., Shanks, W.C., Solow, A.R., 2015. Identification of sulfur sources and isotopic equilibria in submarine hot-springs using multiple sulfur isotopes. Geochim. Cosmochim. Acta 160, 169–187.
Miyashiro, A., 1973. The Troodos ophiolitic complex was probably formed in an island arc. Earth Planet. Sci. Lett. 19, 218–224.
Monecke, T., Petersen, S., Hannington, M.D., 2014. Constraints on water depth of massive sulfide formation: evidence from modern seafloor hydrothermal systems in arc-related settings. Econ. Geol. 109, 2079–2101.
Ohmoto, H., Lasaga, A.C., 1982. Kinetics of reactions between aqueous sulfates and sulfides in hydrothermal systems. Geochim. Cosmochim. Acta 46, 1727–1745.
Ohmoto, H., Mizukami, M., Drummond, S.E., Eldridge, C.S., Pisutha- Arnond, V., Lenagh, T.C., 1983. Chemical Processes of Kuroko Formation: Economic Geology Monographs. pp. 5.
Ono, S., Shanks III, W.C., Rouxel, O.J., Rumble, D., 2007. S-33 constraints on the seawater sulfate contribution in modern seafloor hydrothermal vent sulfides. Geochim. Cosmochim. Acta 71 (5), 1170–1182.
Oudin, E., Constantinou, G., 1984. Black smoker chimney fragments in Cyprus sulphide deposits. Nature 308, 349–353.
Patten, C.G.C., Pitcairn, I.K., Teagle, D.A.H., 2017. Hydrothermal mobilisation of Au and other metals in supra-subduction oceanic crust: insights from the Troodos ophiolite. Ore Geol. Rev. 86, 487–508.
Patten, C.G.C., Pitcairn, I.K., Alt, J.C., Zack, T., Lahaye, Y., Teagle, D.A.H., Markdahl, K., 2019. Metal fluxes during magmatic degassing in the oceanic crust: sulfide mineralisation at ODP site 786B, Izu-Bonin forearc. Min. Dep. 1–21.
Pearce, J.A., Robinson, P.T., 2010. The Troodos ophiolitic complex probably formed in a subduction initiation, slab edge setting. Gondwana Res. 18, 60–81.
Pedersen, L.-E.R., Staudigel, H., McLoughlin, N., Whitehouse, M.J., Strauss, H., 2017. A multiple sulfur isotope study through the volcanic section of the Troodos ophiolite. Chem. Geol. 468, 49–62.
Petersen, S., Herzig, P.M., Hannington, M.D., 2000. Third dimension of a presently forming VMS deposit: TAG hydrothermal mound, Mid-Atlantic Ridge, 26°N. Miner. Deposita 35, 233–259.
Prichard, H.M., Knight, R.D., Fisher, P.C., McDonald, I., Zhou, M.-F., Wang, C.Y., 2013. Distribution of platinum-group elements in magmatic and altered ores in the Jinchuan intrusion, China: an example of selenium remobilization by postmagmatic fluids. Miner. Deposita 48, 767–786.
Regelous, M., Haase, K.M., Freund, S., Keith, M., Weinzierl, C.G., Beier, C., Brandl, P.A., Endres, T., Schmidt, H., 2014. Formation of the Troodos Ophiolite at a triple junction: evidence from trace elements in volcanic glass. Chem. Geol. 386, 66–79.
Richardson, C.J., Cann, J.R., Richards, H.G., Cowan, J.G., 1987. Metal-depleted root zones of the Troodos ore-forming hydrothermal systems, Cyprus. Earth Planet. Sci. Lett. 84, 243–253.
Robertson, A.H.F., 2002. Overview of the genesis and emplacement of Mesozoic ophiolites in the Eastern Mediterranean Tethyan region. In: Strasbourg, France, 28 March-1 April, 1999. Lithos, Eastern Mediterranean Ophiolites: Magmatic Processes and Geodynamic Implications, Held at the 10th Meeting of the European Union of Geosciences 65. pp. 1–67.
Robertson, A.H.F., 1977. Tertiary uplift history of the Troodos massif, Cyprus. GSA Bull. 88, 1763–1772.
Robertson, A.H.F., 1975. Cyprus umbers: basalt-sediment relationships on a Mesozoic ocean ridge. J. Geol. Soc. 131, 511–531.
Robinson, B.W., Kusakabe, M., 1975. Quantitative preparation of sulfur dioxide, for sulfur-34/sulfur-32 analyses, from sulfides by combustion with cuprous oxide. Anal. Chem. 47, 1179–1181.
Robinson, P., Malpas, J., 1990. The Troodos ophiolite of Cyprus: New perspectives on its origin and emplacement. In: OPHIOLITES Oceanic Crustal Analogues, Proceedings of the Symposium "Troodos 1987" The Geological Survey Department, Ministry of Agriculture and Natural Resources, Nicosia, Cyprus.
Rouxel, O., Fouquet, Y., Ludden, J.N., 2004. Subsurface processes at the lucky strike hydrothermal field, Mid- Atlantic ridge: evidence from sulfur, selenium, and iron isotopes 11Associate editor: S. Sheppard. Geochim. Cosmochim. Acta 68, 2295–2311.
Rouxel, O., Ono, S., Alt, J., Rumble, D., Ludden, J., 2008. Sulfur isotope evidence for microbial sulfate reduction in altered oceanic basalts at ODP Site 801. Earth Planet. Sci. Lett. 268 (1-2), 110–123.
Schouten, H., Kelemen, P.B., 2002. Melt viscosity, temperature and transport processes, Troodos ophiolite, Cyprus. Earth Planet. Sci. Lett. 201, 337–352.
Seal, R.R., 2006. Sulfur isotope geochemistry of sulfide minerals. Rev. Mineral. Geochem. 61 (1), 633–677.

Shanks, W.C., Seyfried, W.E., 1987. Stable isotope studies of vent fluids and chimney minerals, southern Juan de Fuca Ridge: sodium metasomatism and seawater sulfate reduction. J. Geophys. Res. Solid Earth 92, 11387–11399.
Sillitoe, R.H., Hannington, M.D., Thompson, J.F.H., 1996. High sulfidation deposits in the volcanogenic massive sulfide environment. Econ. Geol. 91, 204–212.
Smith, J.W., Holwell, D.A., McDonald, I., Boyce, A.J., 2016. The application of S isotopes and S/Se ratios in determining ore- forming processes of magmatic Ni–Cu–PGE sulfide deposits: a cautionary case study from the northern Bushveld Complex. Ore Geol. Rev. 73 (Part 1), 148–174.
Smith, J.W., Holwell, D.A., McDonald, I., 2014. Precious and base metal geochemistry and mineralogy of the Grasvally Norite–pyroxenite–anorthosite (GNPA) member, northern Bushveld Complex, South Africa: implications for a multistage emplacement. Miner. Deposita 49, 667–692.
Staudigel, H., Tauxe, L., Gee, J.S., Bogaard, P., Haspels, J., Kale, G., Leenders, A., Meijer, P., Swaak, B., Tuin, M., Van Soest, M.C., Verdurmen, E.A.T., Zevenhuizen, A., 2000. Geochemistry and intrusive directions in sheeted dikes in the Troodos ophiolite: implications for mid-ocean ridge spreading centers. Geochem. Geophys. Geosyst. 1.
Sun, W., Arculus, R.J., Kamenetsky, V.S., Binns, R.A., 2004. Release of gold-bearing fluids in convergent margin magmas prompted by magnetite crystallization. Nature 431, 975–978.
Tyrrell, T., Zeebe, R.E., 2004. History of carbonate ion concentration over the last 100 million years. Geochim. Cosmochim. Acta 68, 3521–3530.
Varga, R.J., 1991. Modes of extension at oceanic spreading centers: evidence from the Solea graben, Troodos ophiolite, Cyprus. J. Struct. Geol. 13, 517–537.
Varga, R.J., Moores, E.M., 1985. Spreaidng structure of the Troodos ophiolite, Cyprus. Geology 13, 846–850.
Von Damm, K.L., Buttermore, L.G., Oosting, S.E., Bray, A.M., Fornari, D.J., Lilley, M.D., Shanks, W.C., 1997. Direct observation of the evolution of a seafloor “black smoker” from vapor to brine. Earth Planet. Sci. Lett. 149, 101–111.
Von Damm, K.L., Edmond, J.M., Grant, B., Measures, C.I., Walden, B., Weiss, R.F., 1985. Chemistry of submarine hydrothermal solutions at 21 °N, East Pacific Rise. Geochim. Cosmochim. Acta 49, 2197–2220.
Wagner, T., Boyce, A.J., Fallick, A.E., 2002. Laser combustion analysis of δ34S of sulfosalt minerals: determination of the fractionation systematics and some crystal-chemical considerations. Geochim. Cosmochim. Acta 66 (16), 2855–2863.
Williams- Jones, A.E., Heinrich, C.A., 2005. Vapor transport of metals and the formation of magmatic- hydrothermal ore deposits. Econ. Geol. 100, 1287–1312.
Wohlgemuth- Ueberwasser, C.C., Viljoen, F., Petersen, S., Vorster, C., 2015. Distribution and solubility limits of trace elements in hydrothermal black smoker sulfides: an in-situ LA-ICP-MS study. Geochim. Cosmochim. Acta 159, 16–41.
Woodruff, L.G., Shanks, W.C., 1988. Sulfur isotope study of chimney minerals and vent fluids from 21°N, East Pacific Rise: hydrothermal sulfur sources and disequilibrium sulfate reduction. J. Geophys. Res. Solid Earth 93, 4562–4572.
Yang, K., Scott, S.D., 2002. Magmatic degassing of volatiles and ore metals into a hydrothermal system on the modern sea floor of the eastern manus back-arc basin, western pacific. Econ. Geol. 97, 1079–1100.
Yang, K., Scott, S.D., 1996. Possible contribution of a metal-rich magmatic fluid to a seafloor hydrothermal system. Nature 383, 420–423.
Yeats, C.J., Parr, J.M., Binns, R.A., Gemmell, J.B., Scott, S.D., 2014. The SuSu knolls hydrothermal field, Eastern Manus Basin, Papua New Guinea: an active submarine high-sulfidation copper-gold system. Econ. Geol. 109, 2207–2226.